NASA Technical Memorandum 101697

Wind-Tunnel Investigation of a Flush Airdata System at Mach Numbers From 0.7 to 1.4

Terry J. Larson, Timothy R. Moes, and Paul M. Siemers III

April 1990

National Aeronautics and
Space Administration

NASA Technical Memoradum 101697

Wind-Tunnel Investigation of a Flush Airdata System at Mach Numbers From 0.7 to 1.4

Terry J. Larson
Analytical Mechanics Associates, Hampton, Virginia

Timothy R. Moes
Ames Research Center, Dryden Flight Research Facility, Edwards, California

Paul M. Siemers III
Langley Research Center, Hampton, Virginia

1990

National Aeronautics and
Space Administration
Ames Research Center
Dryden Flight Research Facility
Edwards, California 93523-0273

CONTENTS

ABSTRACT	1
INTRODUCTION	1
NOMENCLATURE	2
DESCRIPTION OF MODEL	2
TEST INSTRUMENTATION AND CONDITIONS	3
RESULTS AND DISCUSSION	3
CONCLUDING REMARKS	5
REFERENCES	7
TABLES	8
FIGURES	18

ABSTRACT

Flush pressure orifices installed on the nose section of a 1/7-scale model of the F-14 airplane were evaluated for use as a flush airdata system (FADS). Wind-tunnel tests were conducted in the 11- by 11-ft Unitary Wind Tunnel at NASA Ames Research Center. A full-scale FADS of the same configuration was previously tested using an F-14 aircraft at the Dryden Flight Research Facility of NASA Ames Research Center (Ames-Dryden). These tests, which have been published, are part of a NASA program to assess accuracies of FADS for use on aircraft. The test program also provides data to validate algorithms for the shuttle entry airdata system developed at the NASA Langley Research Center. The wind-tunnel test Mach numbers were 0.73, 0.90, 1.05, 1.20, and 1.39. Angles of attack were varied in 2° increments from −4° to 20°. Sideslip angles were varied in 4° increments from −8° to 8°. Airdata parameters were evaluated for determination of free-stream values of stagnation pressure, static pressure, angle of attack, angle of sideslip, and Mach number. These parameters are, in most cases, the same as the parameters investigated in the flight test program. The basic FADS wind-tunnel data are presented in tabular form. A discussion of the more accurate parameters is included.

INTRODUCTION

For the past several years the Dryden Flight Research Facility of NASA Ames Research Center (Ames-Dryden) has been conducting a wind-tunnel and flight test program to evaluate the accuracy of airdata systems comprised of only pressure orifices flush with the aircraft skin. Such a flush airdata system (FADS) is intended to provide all the conventional airdata quantities, including angle of attack and sideslip, generally provided by pitot-static and flow-angularity-measuring systems on aircraft.

The FADS investigation was begun as support for the shuttle entry airdata sensor (SEADS) program conducted by the NASA Langley Research Center (Siemers and Larson, 1979; Siemers et al., 1988). The SEADS is a FADS-type experimental sensor originally developed to provide airdata for the orbiter at hypersonic speeds. However, early in the program a wind-tunnel test indicated that SEADS could also be accurately applied at lower speeds (Larson and Schweikhard, 1978).

Flight and wind-tunnel data have been obtained at subsonic, transonic, and low supersonic speeds to provide a means for evaluating the use and accuracy of FADS for general flight applications. In addition, these data helped validate the SEADS concept and data algorithms for application at the conditions tested. The subsonic data were obtained using a KC-135 airplane and scale model (Larson et al., 1980; Larson and Siemers, 1980, 1981), and the higher speed data were obtained using an F-14 airplane (Larson et al., 1987). FADS data were also obtained on a 1/7-scale model of the F-14 airplane in the 11- by 11-ft unitary model at the Ames Research Center (*Research Facilities Handbook*, 1982).

The FADS for the F-14 wind-tunnel tests, as for the flight tests, consisted of a spherical nose-cap surface with 11 pressure orifices in a cruciform pattern and additional orifices on the fuselage nose. Wind-tunnel tests were made at Mach 0.60, 0.90, 1.05, 1.20, and 1.39. Angles of attack were varied at 2° increments from −4° to 20°, and sideslip was varied in 4° increments from −8° to 8°. The Mach number and flow-angle ranges for this test were not sufficient for complete calibration over the F-14 flight envelope, but the ranges were sufficient to evaluate the FADS configuration.

The FADS data from the wind-tunnel test are cited in this report. All the data, except repeat runs, are presented in tabular form. Representative data are discussed for application to airdata determination. The criteria used in Larson et al. (1987) for selection of the airdata parameters were also used in the wind-tunnel investigation.

NOMENCLATURE

FADS	flush airdata system
M	free-stream Mach number
p_s	free-stream static pressure, lb/in^2
p_t	free-stream total pressure, lb/in^2
p_{t_2}	stagnation pressure, lb/in^2
p_1 to p_{11}	pressures measured at orifices 1 to 11 on nose cap, lb/in^2
p_{12} to p_{23}	pressures measured at nose section orifices 12 to 23, lb/in^2
$\bar{q}$	free-stream dynamic pressure, lb/in^2
SEADS	shuttle entry airdata system
α	angle of attack, deg
β	angle of sideslip, deg

FADS Pressure Parameters:

AP_{11}	angle-of-attack parameter, nose cap $(p_7 - p_3)/\bar{q}$
AP_{12}	angle-of-attack parameter, nose cap $(p_6 - p_3)/\bar{q}$
AP_{13}	angle-of-attack parameter, nose cap $(p_7 - p_1)/\bar{q}$
AP_{14}	angle-of-attack parameter, nose cap $(p_6 - p_2)/\bar{q}$
AP_{21}	angle-of-attack parameter, station 61 $(p_{14} - p_{12})/\bar{q}$
AP_{31}	angle-of-attack parameter, station 127 $(p_{20} - p_{16})/\bar{q}$
BP_{11}	angle-of-sideslip parameter, nose cap $(p_8 - p_{11})/\bar{q}$
BP_{12}	angle-of-sideslip parameter, nose cap $(p_9 - p_{10})/\bar{q}$
BP_{21}	angle-of-sideslip parameter, station 61 $(p_{15} - p_{13})/\bar{q}$
BP_{32}	angle-of-sideslip parameter, station 127 $[(p_{21} + p_{23}) - (p_{17} + p_{19})]/2\bar{q}$
MP_1	Mach number parameter, p_1/p_4
MP_5	Mach number parameter, $2p_4/(p_{13} + p_{15})$
MP_6	Mach number parameter, $2p_4/(p_{18} + p_{22})$
PP_{22}	static-pressure parameter, station 61 $(p_{12} + p_{14})/2p_s$
PP_{32}	static-pressure parameter, station 127 $(p_{16} + p_{20})/2p_s$
PP_{33}	static-pressure parameter, station 127 $(p_{16} + p_{17} \ldots + p_{23})/8p_s$
PTP_{14}	stagnation-pressure parameter, nose cap, p_4/p_t
PTP_{15}	stagnation-pressure parameter, nose cap, p_5/p_t
PTP_{16}	stagnation-pressure parameter, nose cap, p_6/p_t

DESCRIPTION OF MODEL

The 1/7-scale metal model was equipped with inlets for performance testing. A photograph of the model installed in the wind tunnel is shown in figure 1. The model was considered adequate for testing the FADS concept. However,

a direct comparison of the test results with full-scale test data would be expected to have some significant differences because of configuration differences between the airplane and the model. The fact that the model is wingless should have some effect. However, because the aircraft's wings are well aft of the nose section, the effect may be smaller than those of other configurational differences. For example, the airplane had canardlike surfaces on the fuselage forebody for spin recovery that could have affected the flight FADS measurements. Even though these surfaces were closed for the tests, they were not flush with the airframe. Unlike the model, the aircraft included (1) a gun fairing on the left side of the fuselage, (2) an infrared scanner pod underneath the airplane's nose, and (3) a test airdata probe attached to the nose of the pod. For further details of the airplane, see Larson et al., 1987.

As with the test airplane (Larson et al., 1987), the end of the model's nose was replaced with a sphere-shaped nose cap containing 11 pressure orifices arranged in a cruciform pattern. The geometrical spacing and assigned numbering are shown in figure 2. The sensor is essentially a 1/7-scale replica of the flight test sensor except for the orifice scaling. The model orifice diameters were 0.0134 in., whereas the airplane orifices were 0.0311 in. A smaller model orifice size was avoided because of possible particulate plugging of the orifices.

Two rows of pressure orifices were placed around the model on the fuselage nose aft of the nose cap as shown in figure 2. These locations are at the same relative locations as the test airplane installations. The first row is referred to as being at station 61 and the second row at station 127, which were the orifice distances in in. aft of the airplane's nose apex. Four orifices at station 127 on the airplane were not included on the model. These were orifices 24, 25, 26, and 27 (Larson et al., 1987), located on the bottom of the fuselage. The flight tests indicated that these closely spaced orifices did not provide any additional information not already provided by the other orifices.

TEST INSTRUMENTATION AND CONDITIONS

The FADS wind-tunnel testing was performed in the NASA Ames Research Center's 11- by 11-ft Unitary Wind Tunnel. The model was sting mounted as shown in figure 1. Tables 1 and 2 show the test conditions.

All 23 FADS pressures were measured by 0–15 lb/in^2 transducers having accuracies of 0.25 percent of full scale. Pressures were recorded with a mechanically operated scanning system. The overall accuracy of the pressure measurements were within 0.045 lb/in^2. The tunnel testing characteristics are reported in *Research Facilities Handbook*, 1982.

All test data, with the exception of repeat runs, are presented in tables 1 and 2. The FADS pressures for the repeat runs generally varied less than 0.002 lb/in^2. Table 1 presents the data for 0° angle of sideslip. Note that the first 5 quantities are the test conditions, while the remaining 23 quantities are the ratios of FADS pressure to total pressure. The first group of data are for the various Mach numbers near 0.73. The test Mach number for this group will be referred to as 0.73 even though Mach numbers varied during the angle-of-attack sweep. This group of data is followed by similar groups of data for test Mach numbers of 0.90, 1.05, 1.20, and 1.39. Again, it is noted that Mach numbers varied, in some cases as much as 0.06, from the test values.

Table 2 presents the test data for angles of sideslip of −8°, −4°, 0°, 4°, and 8°. Note that in most cases three angles of attack were obtained for each sideslip angle.

RESULTS AND DISCUSSION

Airdata parameters are shown in figures 3 to 7. These five figures present parameters for determining stagnation pressure, static pressure, angle of attack, angle of sideslip, and Mach number. All of these figures are for 0° angle of sideslip except for figure 6, which shows the variation of the sideslip parameters with angle of sideslip. The data for each figure are plotted against angle of attack or sideslip for each of the five test Mach numbers.

According to the analysis, the three most suitable stagnation-pressure parameters were PTP_{14}, PTP_{15}, and PTP_{16}, calculated using orifices 4, 5, and 6, respectively. These parameters are simply the ratios of the FADS pressures, measured on the nose cap, to total pressure. Ideally, the parameters would not vary with flow angle. Thus, minimal and well-behaved variations of the parameter values with angle of attack were two criteria for selectivity (Larson et al., 1987). Figure 3 shows the variations of the three parameters with angle of attack for the five test Mach numbers. Local zero-flow angles were evidently obtained for PTP_{14} and PTP_{15}, as indicated by the maxima for their curves in figures 3(a) and 3(b), respectively. These maxima correspond within 1 percent of the theoretical ratios of stagnation to total pressure, which are shown in the legends of the figures. This agreement validates both the FADS pressure measurements and the wind-tunnel reference values of Mach number and total pressure.

For subsonic Mach numbers, a reasonably accurate value for stagnation pressure can be obtained without precisely knowing Mach number or angle of attack. At low angles of attack, a value of 0.99 for PTP_{14} will suffice for computing stagnation pressure to within 1 percent of the actual value. For moderate angles of attack (10° to 20°), PTP_{15} would be the most accurate. As indicated by the curves' trends, and as verified by the full-scale flight tests (Larson et al., 1987), PTP_{16} would be best at angles of attack higher than 20°.

If corrections for Mach number and flow angles are applied, any of the three parameters could provide accurate determination of stagnation pressure for this study's test conditions. The requirement for Mach number and angle of attack implies that an iterative calculation scheme is necessary to determine airdata quantities from the FADS. A discussion of iteration methods is given in Larson and Siemers (1980).

The variation of static-pressure parameters for three locations with angle of attack is shown in figure 4. These parameters are the ratios of averaged FADS pressures to the free-stream static pressure. The static-pressure parameters were determined from orifices on the fuselage nose because the pressures there are closer to static pressure than are those sensed on the nose cap. Ideally, the static-pressure parameters should not vary with Mach number or flow angle. However, as expected, the three static-pressure parameters are sensitive to Mach number and angle of attack. Because data were obtained only at five Mach numbers, accurate relationships between the parameters and Mach number cannot be established, as was accomplished in the flight tests which utilized data from accelerations and decelerations. But the effect of angle of attack on the static-pressure parameters were well defined because the data were obtained at 2° increments.

The variations of static-pressure parameters with angle of attack are dependent on Mach number, each parameter having a maximum variation of approximately 0.05 for particular test Mach numbers. Although the larger variations generally occur at the higher Mach numbers, parameter PP_{32} also shows significant variations at the lower two test Mach numbers. The effect of Mach number on the magnitude of the static-pressure parameters can also be evaluated from figure 4. The values of the parameters increase with Mach number, with parameter PP_{22} having the largest change. The variation of the parameters with angle of sideslip (not shown) were a few percent also.

Figure 5 shows the variation of five angle-of-attack parameters with angle of attack. These parameters are the differences between the two FADS pressures divided by the free-stream dynamic pressure. Parameters AP_{11}, AP_{12}, AP_{13}, and AP_{14} use pressures sensed on the nose cap, while AP_{21} and AP_{31} use pressures sensed on the fuselage nose.

Parameter AP_{12} may be the best compromise of the angle-of-attack parameters. The reasons for this choice are (1) its large angle of attack sensitivity (slope of best straight line of parameter with angle of attack), (2) good linearity with angle of attack, and (3) minimum variation of the parameter with Mach number. The variation of the parameter's angle of attack sensitivity for the different Mach numbers ranges from 0.070/deg to 0.078/deg. These sensitivity values are much higher than corresponding sensitivities determined from the fuselage measurements, which vary from 0.022/deg to 0.043/deg. The curves for one of the fuselage parameters, AP_{21}, show good linearity and almost no variation with Mach number. Thus, this parameter would also allow very accurate determination of angle of attack if precise measurements are made of the FADS pressures. The lower angle of attack sensitivity of

parameter AP_{21} dictates that more accurate FADS pressure measurements must be obtained to achieve the same level of angle-of-attack accuracy as parameter AP_{12}.

It is concluded that with proper instrumentation and knowledge of Mach number, all the presented parameters could be used for accurate angle of attack determination. However, although not shown here, angle-of-attack errors as large as 1° could occur if sideslip effects are not accounted for when flying at angles of sideslip near 8°. This is in agreement with the results of Larson et al. (1987).

Figure 6 shows the variation of four angle-of-sideslip parameters with angle of sideslip. These parameters are calculated in the same manner as the angle-of-attack parameters. Parameters BP_{11} and BP_{12} use pressures sensed on the nose cap and the other parameters use pressures sensed on the fuselage nose. All these parameters, using the same orifice locations, were previously investigated in the flight tests reported in Larson et al. (1987), although that study's limited supersonic data were not published. Because the amount of wind-tunnel data taken at any particular angle of attack was small (see table 2), all of the sideslip parameter data (covering an angle-of-attack range from −4° to 18°) are plotted in figure 6. Therefore, angle-of-attack effects, as well as Mach number effects, mask the linearity that would result if the data were plotted for a single angle of attack at constant Mach number.

The sensitivities of the sideslip parameters with angle of sideslip are highest for the nose cap orifices, as they were for the angle-of-attack parameters. The sensitivities for BP_{11}, for example, vary from approximately 0.062/deg to 0.072/deg, depending on the Mach number. These variations can be compared with those of the fuselage nose parameter, BP_{32}, which has sensitivities that vary from 0.026/deg to 0.033/deg. The BP_{32} parameter is judged to be the most accurate of the fuselage nose parameters for ascertaining angle of sideslip.

Figure 7 shows the variation of three Mach number parameters with angle of attack. The first parameter (fig. 7(a)) is the ratio of two pressures, p_1 and p_4, both sensed on the nose cap. The other two parameters (figs. 7(b) and 7(c)) also use ratios of two pressures. However, one pressure is sensed on the nose cap for a near-stagnation-pressure measurement, while the other pressure is sensed on the fuselage nose for a near-static-pressure measurement. For Mach number determination from these parameters, large variations of their values with angle of attack are undesirable. However, all three parameters could be used for determining Mach number, if angle of attack is known, rather than using separate measurements of corrected stagnation pressure and corrected static pressure.

Larson et al. (1987) presented nose cap Mach number parameters using pressure ratios of p_3/p_6 and p_3/p_7. The angles of attack for those data were no greater than approximately 8°. The wind-tunnel data show that these parameters have high sensitivity to angle of attack above 8°. Thus, they are not shown here. The nose cap parameter with the least sensitivity to angle of attack is MP_1. It utilizes pressure p_1 which, because of an instrumentation problem, was not available in the flight program. However, even though MP_1 is the least sensitive of the nose cap parameters to angle of attack, its sensitivity, especially at the higher Mach numbers, is larger than desirable. The other two Mach number parameters, which use fuselage pressures, have much less sensitivity with angle of attack and, as desired, have more variation with Mach number.

In selecting the most accurate parameter for Mach number determination, another factor should be considered in addition to desired sensitivity to Mach number and undesired sensitivity to flow angle. That factor is the importance of the relative magnitude of the pressures in the pressure ratio to the pressure transducer accuracy. However, since all the pressures used in the Mach number parameters were large compared to the accuracies of the pressure measurements, this factor was not significant for these tests. Therefore, parameter MP_6 , which has the largest sensitivity to Mach number and only moderate sensitivity to angle of attack, is the most accurate of the parameters studied for the wind-tunnel test conditions. However, there may be flight conditions for which the measured pressures could be low enough so that the magnitude of the pressures would be important for parameter selectivity.

CONCLUDING REMARKS

A flush airdata system on an F-14 model was tested in the 11- by 11-ft Unitary Wind Tunnel at the NASA Ames Research Center. Pressure orifices were located on a spherical surface of a test nose cap that was blended smoothly to the contours of the airplane's nose section. Orifices were also placed in two rows around the fuselage nose. Measurements were obtained at five Mach numbers from 0.73 to 1.39. Angles of attack were varied in 2° increments from −4° to 20° and angles of sideslip were varied in 4° increments from −8° to 8°.

Nose cap pressures that were investigated for stagnation-pressure determination agreed to within 1 percent of the tunnel-determined stagnation pressure when the local flow angles were zero. This helped validate the FADS pressure measurements as well as verify the wind-tunnel test conditions, especially at supersonic Mach numbers. It was concluded that any of the three pressures investigated could provide accurate determination of stagnation pressure.

The pressure parameters investigated for static-pressure determination were all sensitive to Mach number and angle of attack. The variation of these parameters with angle of attack was well defined. However, the limited number of five test Mach numbers precluded accurately defining the variations with Mach number, as was accomplished in the flight tests that utilized accelerations and decelerations.

One angle-of-attack parameter was judged to be the best compromise between large angle-of-attack sensitivity, linearity with angle of attack, and small variability with Mach number. All of the parameters investigated, including those on the fuselage, could be used for accurate determination of angle of attack with proper instrumentation and knowledge of Mach number and dynamic pressure.

The angle-of-sideslip parameters performed in a manner similar to the angle-of-attack parameters. The sensitivity of the parameters to changes in sideslip was highest for those using nose cap pressures.

Two types of Mach number parameters were investigated: one used the ratio of two nose cap pressures, while the other used the ratio of a nose cap pressure to simulate stagnation pressure and a fuselage pressure to simulate static pressure. The second type of parameter was better because although its sensitivity to angle of attack was less, at the same time its sensitivity to Mach number was much greater.

Ames Research Center
Dryden Flight Research Facility
National Aeronautics and Space Administration
Edwards, California, March 31, 1989

REFERENCES

Larson, Terry J., Stuart G. Flechner, and Paul M. Siemers III, *Wind Tunnel Investigation of an All Flush Orifice Air Data System for a Large Subsonic Aircraft*, NASA TP-1642, 1980.

Larson, Terry J., and William G. Schweikhard, "Use of the Shuttle Entry Air Data Pressure System at Subsonic Speeds," *Proc. Second Biennial Air Data Systems Conference*, May 1978, pp. IV-8-1 to IV-8-7.

Larson, Terry J., and Paul M. Siemers III, "Subsonic Investigation of an All Flush Orifice Air Data System," *Proc. 1980 Air Data Systems Conference*, Colorado Springs, Colorado, May 1980.

Larson, Terry J., and Paul M. Siemers III, *Subsonic Tests of an All-Flush-Pressure-Orifice Air Data System*, NASA TP-1871, 1981.

Larson, Terry J., and Paul M. Siemers III, *Use of Nose Cap and Fuselage Pressure Orifices for Determination of Air Data for Space Shuttle Orbiter Below Supersonic Speeds*, NASA TP-1643, 1980.

Larson, Terry J., Stephen A. Whitmore, L.J. Ehernberger, J. Blair Johnson, and Paul M. Siemers III, *Qualitative Evaluation of a Flush Air Data System at Transonic Speeds and High Angles of Attack*, NASA TP-2716, 1987.

Research Facilities Handbook, NASA Ames Research Center, Moffett Field, California, June 1982.

Siemers, P.M., III, and T.J. Larson, "Space Shuttle Orbiter and Aerodynamic Testing," *J. Spacecraft and Rockets*, vol. 16, no. 4, July-Aug. 1979, p. 223.

Siemers, P.M., III, H. Wolf, and M.W. Henry, "Shuttle Entry Air Data System (SEADS)—Flight Verification of an Advanced Air Data System Concept," AIAA-88-2104, May 1988.

Table 1. Wind-tunnel test data and computed FADS parameters, $\beta = 0°$.

(a) Mach $\approx$ 0.73

Mach	α	p_t	p_s	$\bar{q}$	p_1/p_t	p_2/p_t	p_3/p_t	p_4/p_t	p_5/p_t	p_6/p_t	p_7/p_t	p_8/p_t	p_9/p_t
p_{10}/p_t	p_{11}/p_t	p_{12}/p_t	p_{13}/p_t	p_{14}/p_t	p_{15}/p_t	p_{16}/p_t	p_{17}/p_t	p_{18}/p_t	p_{19}/p_t	p_{20}/p_t	p_{21}/p_t	p_{22}/p_t	p_{23}/p_t
0.735	-4.000	8.080	5.640	2.130	0.917	0.938	0.991	0.988	0.894	0.759	0.738	0.818	0.898
0.895	0.818	0.801	0.706	0.699	0.729	0.747	0.722	0.685	0.663	0.653	0.658	0.686	0.725
0.736	-2.000	8.080	5.639	2.140	0.904	0.924	0.984	0.996	0.916	0.787	0.760	0.829	0.903
0.903	0.828	0.789	0.706	0.710	0.737	0.736	0.719	0.692	0.672	0.660	0.667	0.690	0.721
0.736	0.100	8.078	5.634	2.140	0.888	0.906	0.975	0.999	0.934	0.814	0.780	0.835	0.907
0.909	0.835	0.777	0.705	0.719	0.742	0.728	0.716	0.696	0.682	0.666	0.677	0.695	0.718
0.735	2.000	8.077	5.642	2.130	0.872	0.889	0.963	0.998	0.948	0.838	0.799	0.842	0.910
0.909	0.839	0.766	0.704	0.729	0.744	0.718	0.712	0.700	0.689	0.673	0.685	0.699	0.714
0.733	4.000	8.075	5.649	2.130	0.855	0.870	0.948	0.998	0.964	0.861	0.819	0.845	0.909
0.911	0.843	0.753	0.706	0.740	0.746	0.709	0.708	0.702	0.698	0.682	0.694	0.702	0.712
0.737	8.000	7.892	5.503	2.090	0.821	0.825	0.913	0.992	0.984	0.902	0.858	0.844	0.904
0.906	0.841	0.733	0.702	0.762	0.746	0.693	0.696	0.700	0.711	0.698	0.705	0.695	0.695
0.733	10.000	7.896	5.522	2.080	0.803	0.802	0.891	0.985	0.991	0.922	0.876	0.841	0.899
0.900	0.838	0.722	0.702	0.775	0.740	0.688	0.691	0.697	0.717	0.711	0.714	0.693	0.689
0.731	12.100	7.897	5.534	2.070	0.784	0.777	0.866	0.974	0.997	0.941	0.897	0.834	0.890
0.891	0.831	0.713	0.702	0.791	0.737	0.680	0.685	0.695	0.723	0.725	0.721	0.688	0.684
0.735	14.100	7.892	5.512	2.080	0.762	0.748	0.841	0.961	0.999	0.957	0.913	0.826	0.877
0.879	0.819	0.702	0.695	0.801	0.726	0.673	0.674	0.686	0.725	0.735	0.722	0.681	0.677
0.739	16.000	7.897	5.496	2.100	0.742	0.719	0.812	0.945	0.996	0.967	0.927	0.813	0.865
0.865	0.805	0.689	0.688	0.813	0.716	0.667	0.661	0.674	0.726	0.742	0.724	0.671	0.667
0.736	19.900	7.900	5.513	2.090	0.708	0.670	0.755	0.910	0.990	0.986	0.952	0.787	0.837
0.834	0.773	0.674	0.684	0.838	0.694	0.662	0.649	0.656	0.732	0.768	0.732	0.655	0.654

Table 1. Continued.
(b) Mach $\approx$ 0.90

Mach	α	p_t	p_s	$\bar{q}$	p_1/p_t	p_2/p_t	p_3/p_t	p_4/p_t	p_5/p_t	p_6/p_t	p_7/p_t	p_8/p_t	p_9/p_t
p_{10}/p_t	p_{11}/p_t	p_{12}/p_t	p_{13}/p_t	p_{14}/p_t	p_{15}/p_t	p_{16}/p_t	p_{17}/p_t	p_{18}/p_t	p_{19}/p_t	p_{20}/p_t	p_{21}/p_t	p_{22}/p_t	p_{23}/p_t
0.899	−4.000	7.404	4.383	2.480	0.888	0.916	0.985	0.988	0.874	0.700	0.667	0.768	0.872
0.871	0.770	0.735	0.605	0.606	0.644	0.659	0.629	0.580	0.549	0.533	0.541	0.582	0.630
0.900	−2.000	7.404	4.377	2.480	0.873	0.900	0.977	0.994	0.897	0.735	0.693	0.781	0.878
0.878	0.781	0.721	0.606	0.619	0.654	0.645	0.624	0.589	0.563	0.542	0.555	0.586	0.624
0.900	0.000	7.403	4.377	2.480	0.852	0.878	0.966	0.998	0.917	0.763	0.717	0.789	0.882
0.881	0.786	0.704	0.605	0.632	0.659	0.632	0.617	0.592	0.572	0.551	0.565	0.593	0.620
0.900	2.000	7.410	4.381	2.480	0.832	0.855	0.950	0.999	0.937	0.793	0.740	0.795	0.883
0.886	0.794	0.690	0.605	0.645	0.664	0.618	0.612	0.596	0.583	0.560	0.575	0.595	0.615
0.900	4.000	7.434	4.395	2.490	0.814	0.831	0.934	0.998	0.954	0.822	0.767	0.798	0.883
0.884	0.796	0.674	0.606	0.656	0.667	0.609	0.607	0.599	0.593	0.570	0.586	0.597	0.610
0.903	6.000	7.399	4.362	2.490	0.792	0.803	0.913	0.995	0.969	0.849	0.792	0.800	0.881
0.885	0.796	0.660	0.606	0.673	0.667	0.597	0.600	0.599	0.601	0.582	0.595	0.593	0.600
0.902	8.000	7.400	4.368	2.490	0.769	0.776	0.891	0.990	0.980	0.875	0.814	0.797	0.878
0.880	0.793	0.645	0.604	0.687	0.663	0.584	0.590	0.595	0.611	0.595	0.605	0.593	0.597
0.901	10.000	7.401	4.370	2.480	0.744	0.745	0.863	0.981	0.989	0.899	0.840	0.793	0.870
0.872	0.788	0.632	0.604	0.703	0.660	0.576	0.583	0.594	0.620	0.613	0.612	0.590	0.586
0.896	12.000	7.403	4.397	2.470	0.724	0.716	0.838	0.972	0.996	0.922	0.863	0.790	0.861
0.864	0.784	0.622	0.602	0.723	0.655	0.573	0.577	0.591	0.628	0.627	0.623	0.584	0.579
0.901	14.000	7.404	4.372	2.490	0.701	0.686	0.808	0.957	0.998	0.941	0.883	0.779	0.849
0.852	0.774	0.608	0.594	0.737	0.646	0.564	0.565	0.580	0.633	0.641	0.627	0.576	0.568
0.902	16.100	7.406	4.368	2.490	0.678	0.652	0.775	0.941	0.998	0.956	0.902	0.767	0.836
0.838	0.759	0.597	0.588	0.756	0.635	0.557	0.553	0.571	0.639	0.658	0.635	0.565	0.560
0.901	18.000	7.404	4.373	2.480	0.658	0.622	0.744	0.922	0.997	0.970	0.920	0.753	0.822
0.821	0.745	0.589	0.590	0.771	0.622	0.555	0.547	0.563	0.646	0.676	0.640	0.555	0.554
0.901	20.000	7.397	4.368	2.480	0.639	0.591	0.709	0.902	0.993	0.981	0.937	0.738	0.804
0.804	0.727	0.578	0.574	0.788	0.610	0.551	0.537	0.550	0.650	0.693	0.645	0.543	0.547

Table 1. Continued.

(c) Mach $\approx$ 1.05

Mach	α	p_t	p_s	$\bar{q}$	p_1/p_t	p_2/p_t	p_3/p_t	p_4/p_t	p_5/p_t	p_6/p_t	p_7/p_t	p_8/p_t	p_9/p_t
p_{10}/p_t	p_{11}/p_t	p_{12}/p_t	p_{13}/p_t	p_{14}/p_t	p_{15}/p_t	p_{16}/p_t	p_{17}/p_t	p_{18}/p_t	p_{19}/p_t	p_{20}/p_t	p_{21}/p_t	p_{22}/p_t	p_{23}/p_t
1.048	0.000	7.403	3.696	2.840	0.833	0.863	0.961	0.997	0.912	0.741	0.687	0.766	0.871
0.871	0.765	0.667	0.518	0.587	0.618	0.575	0.560	0.535	0.515	0.487	0.504	0.532	0.560
1.044	2.000	7.401	3.711	2.830	0.813	0.836	0.944	0.999	0.932	0.774	0.712	0.771	0.871
0.873	0.768	0.650	0.520	0.600	0.622	0.561	0.553	0.539	0.523	0.497	0.515	0.535	0.557
1.055	4.000	7.411	3.669	2.860	0.787	0.807	0.925	0.996	0.948	0.801	0.735	0.771	0.868
0.870	0.769	0.630	0.515	0.610	0.619	0.539	0.540	0.534	0.527	0.501	0.519	0.532	0.545
1.050	6.000	7.404	3.688	2.840	0.768	0.782	0.905	0.996	0.963	0.831	0.764	0.776	0.869
0.871	0.771	0.617	0.520	0.630	0.623	0.533	0.536	0.537	0.540	0.518	0.533	0.529	0.539
1.053	8.000	7.403	3.671	2.850	0.738	0.748	0.876	0.989	0.976	0.860	0.790	0.771	0.861
0.864	0.769	0.599	0.516	0.645	0.617	0.513	0.522	0.532	0.548	0.531	0.541	0.523	0.525
1.042	10.100	7.403	3.721	2.830	0.717	0.720	0.853	0.980	0.987	0.888	0.819	0.770	0.856
0.859	0.766	0.585	0.519	0.667	0.617	0.508	0.517	0.532	0.559	0.551	0.553	0.525	0.522
1.034	12.050	7.401	3.755	2.810	0.695	0.690	0.825	0.969	0.993	0.910	0.843	0.766	0.849
0.850	0.761	0.577	0.519	0.687	0.613	0.502	0.508	0.530	0.572	0.570	0.565	0.520	0.514
1.051	14.100	7.408	3.683	2.850	0.667	0.651	0.792	0.956	0.998	0.928	0.864	0.754	0.835
0.837	0.747	0.555	0.508	0.698	0.599	0.482	0.489	0.511	0.572	0.581	0.565	0.497	0.490
1.052	16.000	7.418	3.683	2.850	0.645	0.619	0.762	0.941	0.999	0.947	0.883	0.742	0.824
0.824	0.735	0.543	0.497	0.716	0.589	0.473	0.476	0.500	0.576	0.596	0.571	0.483	0.473
1.046	18.100	7.439	3.721	2.850	0.623	0.585	0.729	0.920	0.998	0.963	0.904	0.730	0.808
0.809	0.720	0.535	0.487	0.737	0.578	0.467	0.464	0.491	0.587	0.617	0.581	0.475	0.460
1.029	20.000	7.407	3.780	2.800	0.608	0.556	0.694	0.899	0.995	0.976	0.924	0.719	0.794
0.792	0.704	0.530	0.497	0.758	0.569	0.466	0.457	0.483	0.598	0.644	0.595	0.468	0.455

Table 1. Continued.
(d) Mach ≈ 1.20

Mach	α	p_t	p_s	$\bar{q}$	p_1/p_t	p_2/p_t	p_3/p_t	p_4/p_t	p_5/p_t	p_6/p_t	p_7/p_t	p_8/p_t	p_9/p_t
p_{10}/p_t	p_{11}/p_t	p_{12}/p_t	p_{13}/p_t	p_{14}/p_t	p_{15}/p_t	p_{16}/p_t	p_{17}/p_t	p_{18}/p_t	p_{19}/p_t	p_{20}/p_t	p_{21}/p_t	p_{22}/p_t	p_{23}/p_t
1.201	−4.000	7.401	3.050	3.080	0.828	0.867	0.966	0.980	0.845	0.618	0.549	0.687	0.826
0.826	0.684	0.638	0.435	0.487	0.537	0.534	0.507	0.451	0.418	0.396	0.407	0.451	0.502
1.201	−2.000	7.399	3.048	3.080	0.803	0.840	0.953	0.987	0.870	0.652	0.574	0.694	0.831
0.830	0.691	0.617	0.440	0.499	0.543	0.517	0.498	0.456	0.428	0.404	0.419	0.455	0.496
1.203	0.000	7.400	3.042	3.080	0.778	0.813	0.939	0.990	0.891	0.685	0.603	0.701	0.833
0.832	0.698	0.601	0.443	0.513	0.550	0.501	0.490	0.461	0.439	0.414	0.433	0.458	0.487
1.202	2.000	7.400	3.045	3.080	0.753	0.784	0.919	0.991	0.913	0.717	0.631	0.705	0.834
0.835	0.701	0.583	0.446	0.529	0.554	0.484	0.482	0.465	0.452	0.426	0.445	0.459	0.478
1.198	4.000	7.401	3.059	3.070	0.726	0.751	0.898	0.988	0.931	0.751	0.663	0.708	0.832
0.834	0.705	0.565	0.447	0.545	0.555	0.469	0.474	0.465	0.462	0.438	0.458	0.462	0.473
1.195	6.000	7.401	3.070	3.070	0.701	0.721	0.874	0.986	0.950	0.786	0.698	0.714	0.830
0.834	0.708	0.548	0.448	0.565	0.556	0.459	0.466	0.466	0.475	0.454	0.470	0.462	0.467
1.190	8.000	7.402	3.094	3.060	0.675	0.688	0.848	0.980	0.964	0.821	0.734	0.715	0.828
0.829	0.707	0.532	0.449	0.586	0.558	0.446	0.459	0.467	0.487	0.473	0.485	0.460	0.457
1.197	10.000	7.437	3.078	3.090	0.643	0.647	0.817	0.971	0.973	0.844	0.758	0.705	0.815
0.820	0.700	0.510	0.432	0.600	0.546	0.429	0.441	0.459	0.494	0.486	0.491	0.451	0.440
1.194	12.000	7.410	3.079	3.070	0.618	0.613	0.789	0.959	0.982	0.873	0.788	0.701	0.810
0.814	0.697	0.501	0.435	0.624	0.545	0.422	0.432	0.455	0.505	0.505	0.502	0.444	0.431
1.186	14.100	7.396	3.106	3.060	0.598	0.582	0.759	0.946	0.989	0.903	0.822	0.702	0.802
0.806	0.693	0.491	0.437	0.646	0.540	0.414	0.425	0.449	0.517	0.525	0.512	0.440	0.425
1.176	16.000	7.400	3.149	3.050	0.582	0.553	0.732	0.931	0.991	0.926	0.851	0.698	0.795
0.797	0.689	0.483	0.439	0.669	0.532	0.411	0.415	0.444	0.528	0.546	0.525	0.431	0.415
1.163	18.050	7.400	3.202	3.030	0.566	0.521	0.700	0.914	0.993	0.945	0.876	0.688	0.782
0.784	0.680	0.476	0.441	0.693	0.524	0.407	0.408	0.437	0.540	0.571	0.535	0.424	0.412
1.144	20.100	7.401	3.278	3.010	0.559	0.499	0.674	0.894	0.991	0.965	0.905	0.684	0.774
0.775	0.673	0.477	0.448	0.723	0.522	0.410	0.404	0.433	0.555	0.599	0.551	0.420	0.404

Table 1. Concluded.

(e) Mach $\approx$ 1.39

Mach	α	p_t	p_s	$\bar{q}$	p_1/p_t	p_2/p_t	p_3/p_t	p_4/p_t	p_5/p_t	p_6/p_t	p_7/p_t	p_8/p_t	p_9/p_t
p_{10}/p_t	p_{11}/p_t	p_{12}/p_t	p_{13}/p_t	p_{14}/p_t	p_{15}/p_t	p_{16}/p_t	p_{17}/p_t	p_{18}/p_t	p_{19}/p_t	p_{20}/p_t	p_{21}/p_t	p_{22}/p_t	p_{23}/p_t
1.389	−4.000	7.388	2.358	3.180	0.718	0.768	0.912	0.950	0.807	0.552	0.368	0.578	0.760
0.754	0.561	0.548	0.335	0.392	0.447	0.451	0.424	0.364	0.334	0.313	0.325	0.364	0.413
1.390	−2.000	7.391	2.357	3.190	0.689	0.739	0.898	0.955	0.830	0.577	0.394	0.575	0.759
0.758	0.564	0.528	0.338	0.404	0.452	0.434	0.418	0.372	0.345	0.321	0.337	0.368	0.407
1.389	0.000	7.388	2.358	3.180	0.656	0.703	0.877	0.956	0.850	0.601	0.427	0.574	0.757
0.758	0.563	0.504	0.339	0.418	0.454	0.417	0.406	0.375	0.358	0.332	0.350	0.374	0.401
1.388	2.000	7.389	2.361	3.180	0.623	0.667	0.855	0.953	0.867	0.629	0.467	0.573	0.753
0.756	0.565	0.486	0.342	0.432	0.458	0.399	0.395	0.376	0.367	0.343	0.361	0.375	0.393
1.387	4.000	7.389	2.364	3.180	0.593	0.636	0.836	0.956	0.886	0.658	0.507	0.573	0.752
0.756	0.568	0.471	0.349	0.449	0.460	0.385	0.388	0.379	0.378	0.355	0.372	0.374	0.383
1.387	6.000	7.393	2.365	3.190	0.555	0.594	0.808	0.951	0.903	0.693	0.551	0.573	0.747
0.753	0.569	0.451	0.349	0.471	0.463	0.371	0.377	0.379	0.390	0.369	0.385	0.371	0.375
1.385	8.000	7.395	2.374	3.190	0.519	0.556	0.780	0.944	0.919	0.725	0.593	0.574	0.743
0.748	0.568	0.431	0.351	0.487	0.460	0.355	0.365	0.376	0.400	0.386	0.398	0.371	0.366
1.381	10.150	7.402	2.388	3.190	0.484	0.517	0.753	0.938	0.934	0.758	0.632	0.573	0.738
0.744	0.569	0.416	0.349	0.512	0.457	0.346	0.355	0.372	0.413	0.404	0.411	0.364	0.353
1.380	12.050	7.403	2.393	3.190	0.449	0.487	0.728	0.926	0.942	0.787	0.667	0.573	0.734
0.739	0.569	0.402	0.350	0.531	0.451	0.335	0.345	0.366	0.423	0.421	0.420	0.357	0.344
1.375	14.150	7.402	2.408	3.190	0.415	0.453	0.699	0.913	0.948	0.817	0.704	0.572	0.725
0.732	0.567	0.387	0.351	0.554	0.442	0.324	0.332	0.359	0.430	0.439	0.427	0.354	0.334
1.371	16.100	7.398	2.421	3.190	0.398	0.425	0.673	0.901	0.956	0.846	0.739	0.573	0.721
0.723	0.568	0.379	0.356	0.577	0.437	0.318	0.322	0.354	0.440	0.459	0.439	0.346	0.322
1.365	18.100	7.402	2.444	3.190	0.384	0.401	0.646	0.886	0.959	0.872	0.772	0.572	0.713
0.716	0.565	0.368	0.364	0.601	0.428	0.311	0.308	0.343	0.451	0.480	0.450	0.339	0.307
1.357	20.000	7.401	2.470	3.180	0.376	0.380	0.617	0.867	0.960	0.895	0.805	0.572	0.706
0.707	0.564	0.361	0.370	0.626	0.421	0.309	0.298	0.337	0.460	0.502	0.463	0.335	0.299

Table 2. Wind-tunnel test data and computed FADS parameters for various angles of sideslip.
(a) Mach ≈ 0.73

β	Mach	α	p_t	p_s	$\bar{q}$	p_1/p_t	p_2/p_t	p_3/p_t	p_4/p_t	p_5/p_t	p_6/p_t	p_7/p_t	p_8/p_t	p_9/p_t
	p_{10}/p_t	p_{11}/p_t	p_{12}/p_t	p_{13}/p_t	p_{14}/p_t	p_{15}/p_t	p_{16}/p_t	p_{17}/p_t	p_{18}/p_t	p_{19}/p_t	p_{20}/p_t	p_{21}/p_t	p_{22}/p_t	p_{23}/p_t
0.060	0.735	−3.990	8.064	5.630	2.130	0.918	0.941	0.991	0.989	0.897	0.763	0.741	0.819	0.900
	0.898	0.819	0.803	0.707	0.701	0.731	0.750	0.726	0.687	0.666	0.657	0.660	0.686	0.724
0.010	0.736	0.070	8.078	5.634	2.140	0.888	0.906	0.975	0.999	0.934	0.814	0.780	0.835	0.907
	0.909	0.835	0.777	0.705	0.719	0.742	0.728	0.716	0.696	0.682	0.666	0.677	0.695	0.718
3.990	0.754	10.040	7.901	5.420	2.160	0.786	0.786	0.880	0.978	0.986	0.917	0.868	0.867	0.925
	0.855	0.791	0.702	0.689	0.763	0.753	0.665	0.667	0.667	0.685	0.694	0.716	0.699	0.685
4.000	0.735	14.010	7.896	5.511	2.090	0.757	0.745	0.836	0.958	0.993	0.950	0.908	0.860	0.910
	0.840	0.782	0.695	0.693	0.797	0.750	0.667	0.670	0.669	0.699	0.728	0.741	0.701	0.677
4.000	0.733	18.060	7.899	5.525	2.080	0.721	0.693	0.782	0.928	0.992	0.975	0.939	0.835	0.885
	0.814	0.756	0.681	0.688	0.826	0.731	0.663	0.660	0.654	0.706	0.758	0.757	0.680	0.657
8.010	0.736	2.010	7.903	5.515	2.090	0.854	0.871	0.946	0.983	0.932	0.821	0.785	0.906	0.967
	0.823	0.761	0.750	0.701	0.713	0.791	0.702	0.672	0.672	0.670	0.660	0.692	0.734	0.737
7.990	0.736	5.980	7.902	5.514	2.090	0.817	0.830	0.914	0.979	0.957	0.864	0.822	0.911	0.965
	0.821	0.764	0.725	0.698	0.734	0.793	0.685	0.672	0.670	0.673	0.676	0.718	0.741	0.723
8.000	0.734	17.800	7.906	5.526	2.080	0.708	0.685	0.777	0.919	0.981	0.961	0.924	0.868	0.913
	0.772	0.721	0.673	0.685	0.811	0.756	0.650	0.665	0.646	0.676	0.744	0.776	0.701	0.650
−4.010	0.736	10.010	7.903	5.515	2.090	0.795	0.796	0.886	0.979	0.988	0.921	0.873	0.803	0.858
	0.931	0.871	0.715	0.699	0.772	0.718	0.680	0.693	0.713	0.731	0.706	0.693	0.698	0.680
−4.000	0.731	14.010	7.904	5.538	2.070	0.762	0.745	0.839	0.957	0.995	0.952	0.909	0.790	0.841
	0.912	0.855	0.698	0.699	0.801	0.710	0.672	0.676	0.706	0.747	0.733	0.701	0.667	0.674
−4.000	0.724	17.970	7.903	5.574	2.050	0.726	0.697	0.783	0.925	0.991	0.976	0.936	0.769	0.817
	0.884	0.827	0.683	0.688	0.826	0.688	0.665	0.655	0.684	0.754	0.752	0.699	0.661	0.670

Table 2. Continued.

(b) Mach ≈ 0.90

β	Mach	α	p_t	p_s	$\bar{q}$	p_1/p_t	p_2/p_t	p_3/p_t	p_4/p_t	p_5/p_t	p_6/p_t	p_7/p_t	p_8/p_t	p_9/p_t
	p_{10}/p_t	p_{11}/p_t	p_{12}/p_t	p_{13}/p_t	p_{14}/p_t	p_{15}/p_t	p_{16}/p_t	p_{17}/p_t	p_{18}/p_t	p_{19}/p_t	p_{20}/p_t	p_{21}/p_t	p_{22}/p_t	p_{23}/p_t
−0.020	0.899	−4.000	7.404	4.383	2.480	0.888	0.916	0.985	0.988	0.874	0.700	0.667	0.768	0.872
	0.871	0.770	0.735	0.605	0.606	0.644	0.659	0.629	0.580	0.549	0.533	0.541	0.582	0.630
0.030	0.900	−0.040	7.403	4.375	2.480	0.852	0.878	0.966	0.996	0.917	0.764	0.716	0.788	0.882
	0.883	0.787	0.703	0.604	0.629	0.658	0.630	0.618	0.593	0.573	0.550	0.565	0.593	0.621
4.000	0.900	10.080	7.399	4.377	2.480	0.739	0.739	0.860	0.978	0.985	0.897	0.838	0.838	0.911
	0.826	0.744	0.627	0.605	0.702	0.690	0.572	0.573	0.576	0.597	0.612	0.637	0.610	0.593
4.020	0.900	14.070	7.398	4.373	2.480	0.693	0.679	0.803	0.952	0.994	0.937	0.880	0.822	0.889
	0.803	0.725	0.603	0.595	0.733	0.675	0.559	0.563	0.563	0.604	0.640	0.657	0.602	0.570
4.040	0.901	17.960	7.399	4.371	2.480	0.649	0.616	0.741	0.919	0.995	0.967	0.918	0.797	0.863
	0.777	0.698	0.585	0.585	0.769	0.654	0.550	0.550	0.544	0.612	0.673	0.673	0.579	0.546
8.010	0.899	1.980	7.401	4.381	2.480	0.813	0.838	0.932	0.982	0.920	0.778	0.727	0.877	0.957
	0.782	0.699	0.673	0.603	0.627	0.724	0.602	0.562	0.558	0.555	0.546	0.590	0.648	0.651
8.020	0.901	6.010	7.401	4.373	2.480	0.771	0.787	0.897	0.980	0.950	0.832	0.777	0.885	0.957
	0.779	0.703	0.643	0.605	0.655	0.729	0.581	0.563	0.559	0.564	0.570	0.623	0.644	0.626
7.880	0.901	17.600	7.404	4.372	2.490	0.640	0.612	0.740	0.912	0.981	0.949	0.900	0.837	0.898
	0.731	0.658	0.575	0.739	0.753	0.689	0.539	0.553	0.532	0.575	0.659	0.697	0.607	0.540
−3.990	0.899	9.980	7.389	4.372	2.480	0.742	0.740	0.859	0.976	0.986	0.897	0.836	0.750	0.823
	0.913	0.833	0.628	0.606	0.704	0.634	0.575	0.590	0.618	0.641	0.609	0.592	0.571	0.580
−4.010	0.899	13.890	7.402	4.381	2.480	0.697	0.682	0.804	0.952	0.995	0.937	0.878	0.737	0.805
	0.892	0.817	0.606	0.598	0.734	0.620	0.560	0.566	0.606	0.660	0.639	0.600	0.555	0.567
−4.000	0.904	17.920	7.415	4.368	2.500	0.654	0.615	0.740	0.916	0.994	0.967	0.914	0.710	0.776
	0.860	0.786	0.583	0.587	0.767	0.595	0.549	0.542	0.583	0.674	0.671	0.606	0.531	0.550
−8.030	0.902	2.010	7.400	4.367	2.490	0.812	0.834	0.931	0.982	0.918	0.782	0.723	0.699	0.781
	0.958	0.877	0.671	0.608	0.631	0.609	0.601	0.647	0.648	0.599	0.544	0.552	0.556	0.562
−8.000	0.900	6.010	7.392	4.372	2.480	0.771	0.785	0.896	0.977	0.950	0.836	0.772	0.709	0.779
	0.957	0.880	0.645	0.608	0.661	0.615	0.580	0.624	0.651	0.632	0.570	0.561	0.558	0.566
−8.350	0.899	17.530	7.404	4.385	2.480	0.643	0.612	0.735	0.905	0.978	0.950	0.897	0.663	0.722
	0.898	0.833	0.575	0.590	0.755	0.573	0.539	0.536	0.618	0.705	0.659	0.567	0.521	0.559

Table 2. Continued.
(c) Mach ≈ 1.05

β	Mach	α	p_t	p_s	$\bar{q}$	p_1/p_t	p_2/p_t	p_3/p_t	p_4/p_t	p_5/p_t	p_6/p_t	p_7/p_t	p_8/p_t	p_9/p_t
	p_{10}/p_t	p_{11}/p_t	p_{12}/p_t	p_{13}/p_t	p_{14}/p_t	p_{15}/p_t	p_{16}/p_t	p_{17}/p_t	p_{18}/p_t	p_{19}/p_t	p_{20}/p_t	p_{21}/p_t	p_{22}/p_t	p_{23}/p_t
−0.050	1.048	−0.030	7.403	3.696	2.840	0.833	0.863	0.961	0.997	0.912	0.741	0.687	0.766	0.871
	0.871	0.765	0.667	0.518	0.587	0.618	0.575	0.560	0.535	0.515	0.487	0.504	0.532	0.560
3.990	1.054	10.050	7.384	3.657	2.850	0.709	0.711	0.846	0.977	0.984	0.883	0.815	0.814	0.899
	0.810	0.716	0.577	0.510	0.659	0.647	0.499	0.500	0.503	0.532	0.547	0.574	0.544	0.522
4.000	1.050	14.060	7.416	3.693	2.850	0.660	0.646	0.788	0.950	0.993	0.924	0.860	0.798	0.877
	0.788	0.697	0.549	0.504	0.693	0.629	0.479	0.483	0.486	0.539	0.577	0.594	0.527	0.494
3.990	1.045	18.060	7.444	3.731	2.850	0.615	0.579	0.725	0.916	0.993	0.958	0.903	0.776	0.851
	0.760	0.671	0.531	0.487	0.733	0.610	0.464	0.465	0.466	0.551	0.616	0.616	0.507	0.464
7.990	1.048	1.990	7.370	3.679	2.830	0.793	0.819	0.927	0.983	0.915	0.759	0.700	0.861	0.950
	0.765	0.671	0.633	0.516	0.586	0.689	0.543	0.500	0.494	0.493	0.482	0.534	0.592	0.598
7.990	1.052	6.010	7.407	3.677	2.850	0.746	0.765	0.885	0.977	0.944	0.814	0.750	0.864	0.946
	0.761	0.669	0.597	0.510	0.613	0.689	0.512	0.493	0.491	0.496	0.506	0.564	0.590	0.569
7.990	1.049	10.050	7.413	3.695	2.850	0.696	0.701	0.836	0.962	0.968	0.869	0.803	0.858	0.935
	0.752	0.665	0.568	0.511	0.648	0.680	0.488	0.489	0.486	0.503	0.535	0.595	0.582	0.536
−4.000	1.050	10.010	7.406	3.686	2.850	0.711	0.712	0.848	0.976	0.984	0.884	0.814	0.722	0.808
	0.902	0.810	0.581	0.518	0.662	0.586	0.498	0.520	0.554	0.581	0.544	0.527	0.492	0.502
−3.990	1.052	14.040	7.422	3.684	2.860	0.661	0.645	0.786	0.950	0.993	0.924	0.859	0.706	0.786
	0.878	0.790	0.551	0.508	0.694	0.567	0.473	0.490	0.537	0.597	0.575	0.535	0.471	0.482
−3.990	1.043	18.050	7.427	3.731	2.840	0.619	0.580	0.723	0.915	0.994	0.959	0.901	0.686	0.761
	0.849	0.764	0.532	0.494	0.735	0.548	0.464	0.463	0.522	0.620	0.616	0.548	0.451	0.465
−7.990	1.049	2.000	7.404	3.690	2.840	0.791	0.817	0.926	0.982	0.916	0.763	0.694	0.672	0.766
	0.951	0.861	0.631	0.518	0.588	0.564	0.539	0.590	0.594	0.546	0.479	0.485	0.485	0.491
−8.000	1.052	5.990	7.404	3.679	2.850	0.745	0.761	0.885	0.975	0.944	0.819	0.747	0.677	0.760
	0.947	0.862	0.600	0.517	0.616	0.566	0.508	0.560	0.592	0.575	0.504	0.491	0.485	0.491
−7.990	1.050	10.010	7.402	3.684	2.840	0.697	0.700	0.835	0.961	0.967	0.872	0.799	0.672	0.749
	0.936	0.853	0.568	0.517	0.652	0.560	0.485	0.529	0.585	0.602	0.534	0.499	0.474	0.487

Table 2. Continued.

(d) Mach ≈ 1.20

β	Mach	α	p_t	p_s	$\bar{q}$	p_1/p_t	p_2/p_t	p_3/p_t	p_4/p_t	p_5/p_t	p_6/p_t	p_7/p_t	p_8/p_t	p_9/p_t
	p_{10}/p_t	p_{11}/p_t	p_{12}/p_t	p_{13}/p_t	p_{14}/p_t	p_{15}/p_t	p_{16}/p_t	p_{17}/p_t	p_{18}/p_t	p_{19}/p_t	p_{20}/p_t	p_{21}/p_t	p_{22}/p_t	p_{23}/p_t
−0.040	1.201	−3.990	7.401	3.050	3.080	0.828	0.867	0.966	0.980	0.845	0.618	0.549	0.687	0.826
	0.826	0.684	0.638	0.435	0.487	0.537	0.534	0.507	0.451	0.418	0.396	0.407	0.451	0.502
−0.010	1.203	−0.020	7.400	3.042	3.080	0.778	0.813	0.939	0.990	0.891	0.685	0.603	0.701	0.833
	0.832	0.698	0.601	0.443	0.513	0.550	0.501	0.490	0.461	0.439	0.414	0.433	0.458	0.487
3.980	1.197	10.020	7.415	3.071	3.080	0.641	0.647	0.815	0.966	0.970	0.842	0.758	0.763	0.868
	0.768	0.647	0.508	0.435	0.599	0.583	0.421	0.426	0.430	0.466	0.482	0.512	0.478	0.452
4.000	1.181	14.070	7.397	3.128	3.050	0.595	0.582	0.756	0.943	0.985	0.900	0.821	0.753	0.850
	0.754	0.642	0.488	0.444	0.643	0.576	0.412	0.419	0.427	0.487	0.524	0.542	0.469	0.431
4.010	1.157	17.970	7.402	3.225	3.020	0.560	0.523	0.701	0.910	0.990	0.942	0.874	0.742	0.831
	0.735	0.628	0.477	0.449	0.692	0.562	0.404	0.410	0.415	0.506	0.569	0.570	0.458	0.411
8.010	1.206	2.000	7.384	3.021	3.080	0.732	0.765	0.901	0.972	0.895	0.702	0.620	0.808	0.920
	0.715	0.586	0.563	0.434	0.508	0.622	0.464	0.422	0.412	0.414	0.410	0.467	0.524	0.528
8.030	1.198	6.010	7.407	3.061	3.080	0.685	0.709	0.861	0.970	0.933	0.774	0.690	0.821	0.923
	0.718	0.596	0.534	0.440	0.549	0.631	0.437	0.420	0.416	0.430	0.442	0.504	0.522	0.498
8.150	1.144	18.110	7.411	3.283	3.010	0.551	0.521	0.695	0.898	0.977	0.931	0.867	0.794	0.870
	0.681	0.581	0.472	0.456	0.687	0.609	0.400	0.414	0.403	0.472	0.566	0.608	0.501	0.414
−3.990	1.196	10.080	7.473	3.097	3.100	0.640	0.645	0.813	0.966	0.972	0.848	0.761	0.656	0.765
	0.871	0.757	0.506	0.440	0.603	0.517	0.429	0.453	0.491	0.522	0.484	0.469	0.425	0.426
−4.020	1.180	14.110	7.500	3.172	3.090	0.599	0.580	0.758	0.941	0.986	0.904	0.824	0.653	0.751
	0.855	0.750	0.488	0.452	0.649	0.509	0.415	0.430	0.485	0.550	0.524	0.485	0.414	0.416
−3.990	1.157	18.040	7.535	3.283	3.080	0.565	0.521	0.698	0.909	0.991	0.945	0.877	0.641	0.736
	0.829	0.733	0.474	0.448	0.696	0.496	0.410	0.410	0.473	0.577	0.570	0.506	0.404	0.407
−8.000	1.201	−2.01	7.396	3.047	3.08	0.786	0.824	0.936	0.969	0.851	0.645	0.556	0.582	0.717
	0.92	0.801	0.604	0.438	0.489	0.484	0.504	0.555	0.525	0.449	0.392	0.407	0.408	0.42
−7.990	1.199	6	7.415	3.064	3.08	0.682	0.704	0.858	0.967	0.931	0.776	0.684	0.601	0.714
	0.923	0.813	0.53	0.442	0.553	0.497	0.445	0.498	0.532	0.518	0.44	0.427	0.412	0.419
−7.730	1.144	18.6	7.433	3.294	3.02	0.552	0.511	0.681	0.888	0.976	0.941	0.874	0.594	0.68
	0.86	0.775	0.468	0.456	0.699	0.473	0.406	0.404	0.508	0.614	0.574	0.475	0.385	0.411

Table 2. Concluded.

(e) Mach ≈ 1.39

β	Mach	α	p_t	p_s	$\bar{q}$	p_1/p_t	p_2/p_t	p_3/p_t	p_4/p_t	p_5/p_t	p_6/p_t	p_7/p_t	p_8/p_t	p_9/p_t
	p_{10}/p_t	p_{11}/p_t	p_{12}/p_t	p_{13}/p_t	p_{14}/p_t	p_{15}/p_t	p_{16}/p_t	p_{17}/p_t	p_{18}/p_t	p_{19}/p_t	p_{20}/p_t	p_{21}/p_t	p_{22}/p_t	p_{23}/p_t
0.050	1.389	−4.000	7.388	2.358	3.180	0.718	0.768	0.912	0.950	0.807	0.552	0.368	0.578	0.760
	0.754	0.561	0.548	0.335	0.392	0.447	0.451	0.424	0.364	0.334	0.313	0.325	0.364	0.413
−0.020	1.389	−0.010	7.388	2.358	3.180	0.656	0.703	0.877	0.956	0.850	0.601	0.427	0.574	0.757
	0.758	0.563	0.504	0.339	0.418	0.454	0.417	0.406	0.375	0.358	0.332	0.350	0.374	0.401
3.990	1.381	10.030	7.396	2.386	3.190	0.484	0.520	0.751	0.934	0.929	0.755	0.631	0.637	0.791
	0.690	0.506	0.413	0.349	0.505	0.489	0.337	0.340	0.345	0.385	0.400	0.431	0.393	0.366
4.010	1.374	14.040	7.398	2.412	3.190	0.421	0.456	0.699	0.913	0.948	0.816	0.704	0.636	0.778
	0.681	0.511	0.389	0.359	0.550	0.481	0.319	0.326	0.336	0.399	0.437	0.460	0.382	0.338
3.990	1.362	17.950	7.401	2.454	3.190	0.383	0.403	0.646	0.883	0.957	0.869	0.770	0.633	0.762
	0.667	0.511	0.366	0.363	0.596	0.465	0.305	0.310	0.317	0.411	0.478	0.486	0.371	0.308
8.010	1.388	1.980	7.402	2.367	3.190	0.620	0.665	0.848	0.944	0.855	0.623	0.472	0.702	0.855
	0.649	0.439	0.478	0.341	0.420	0.534	0.383	0.339	0.329	0.335	0.328	0.382	0.436	0.442
8.010	1.385	6.010	7.400	2.374	3.190	0.554	0.596	0.800	0.937	0.889	0.682	0.551	0.705	0.850
	0.642	0.439	0.440	0.344	0.454	0.539	0.351	0.332	0.329	0.345	0.357	0.421	0.434	0.412
8.220	1.359	18.000	7.395	2.462	3.180	0.382	0.405	0.643	0.873	0.945	0.860	0.767	0.696	0.811
	0.614	0.456	0.362	0.359	0.589	0.508	0.295	0.311	0.298	0.373	0.470	0.520	0.410	0.306
−4.010	1.383	10.050	7.401	2.383	3.190	0.482	0.517	0.749	0.932	0.928	0.759	0.631	0.512	0.686
	0.793	0.631	0.411	0.357	0.507	0.423	0.340	0.365	0.403	0.439	0.402	0.384	0.341	0.340
−3.990	1.377	14.030	7.400	2.402	3.190	0.413	0.454	0.697	0.910	0.945	0.814	0.699	0.512	0.673
	0.779	0.626	0.387	0.362	0.551	0.412	0.323	0.338	0.389	0.463	0.437	0.398	0.325	0.324
−3.990	1.365	18.040	7.400	2.442	3.190	0.378	0.401	0.641	0.880	0.955	0.870	0.770	0.516	0.661
	0.762	0.622	0.362	0.365	0.598	0.392	0.307	0.303	0.373	0.486	0.476	0.411	0.313	0.309
−8.010	1.388	1.99	7.399	2.366	3.19	0.613	0.658	0.842	0.942	0.854	0.629	0.477	0.452	0.645
	0.853	0.693	0.467	0.339	0.418	0.394	0.387	0.44	0.443	0.396	0.331	0.331	0.326	0.333
−7.990	1.384	5.99	7.399	2.377	3.19	0.545	0.587	0.797	0.934	0.889	0.69	0.551	0.443	0.637
	0.85	0.696	0.432	0.344	0.455	0.4	0.356	0.409	0.442	0.43	0.358	0.345	0.325	0.327
−7.760	1.359	18.51	7.396	2.461	3.18	0.366	0.397	0.629	0.865	0.947	0.871	0.775	0.464	0.611
	0.801	0.676	0.353	0.373	0.601	0.367	0.299	0.298	0.409	0.523	0.479	0.375	0.291	0.308

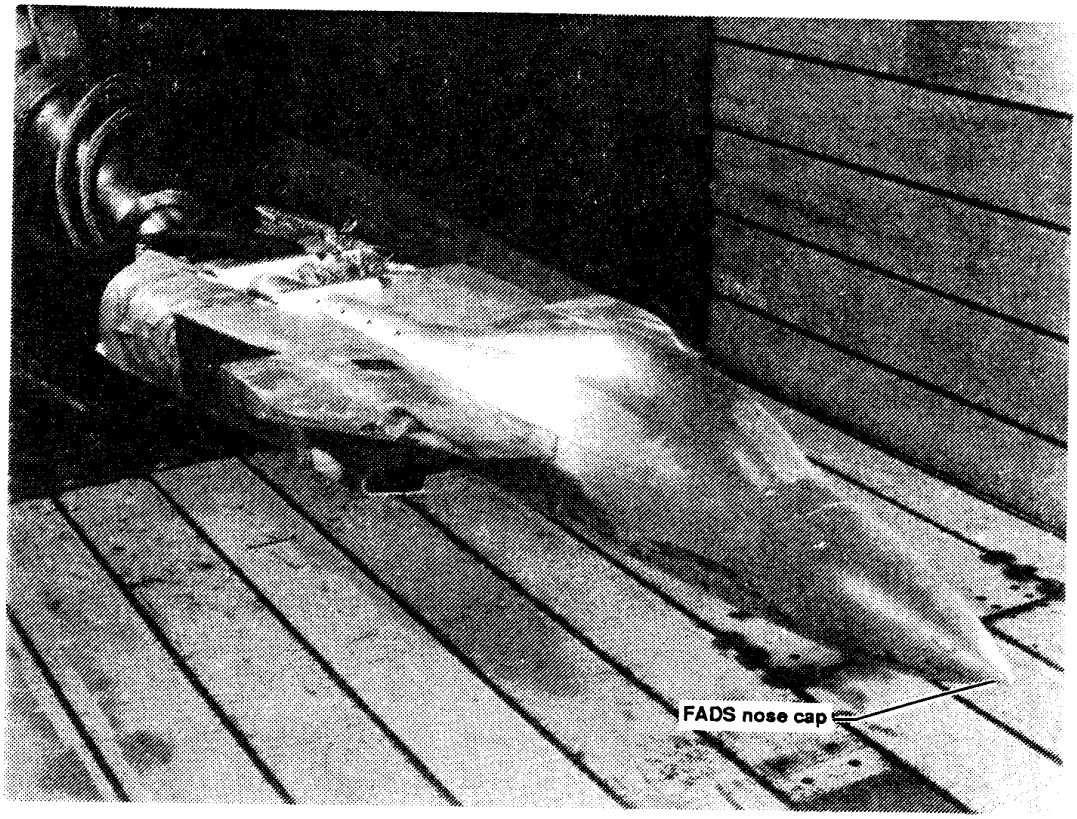

9958

Figure 1. F-14 wind-tunnel model.

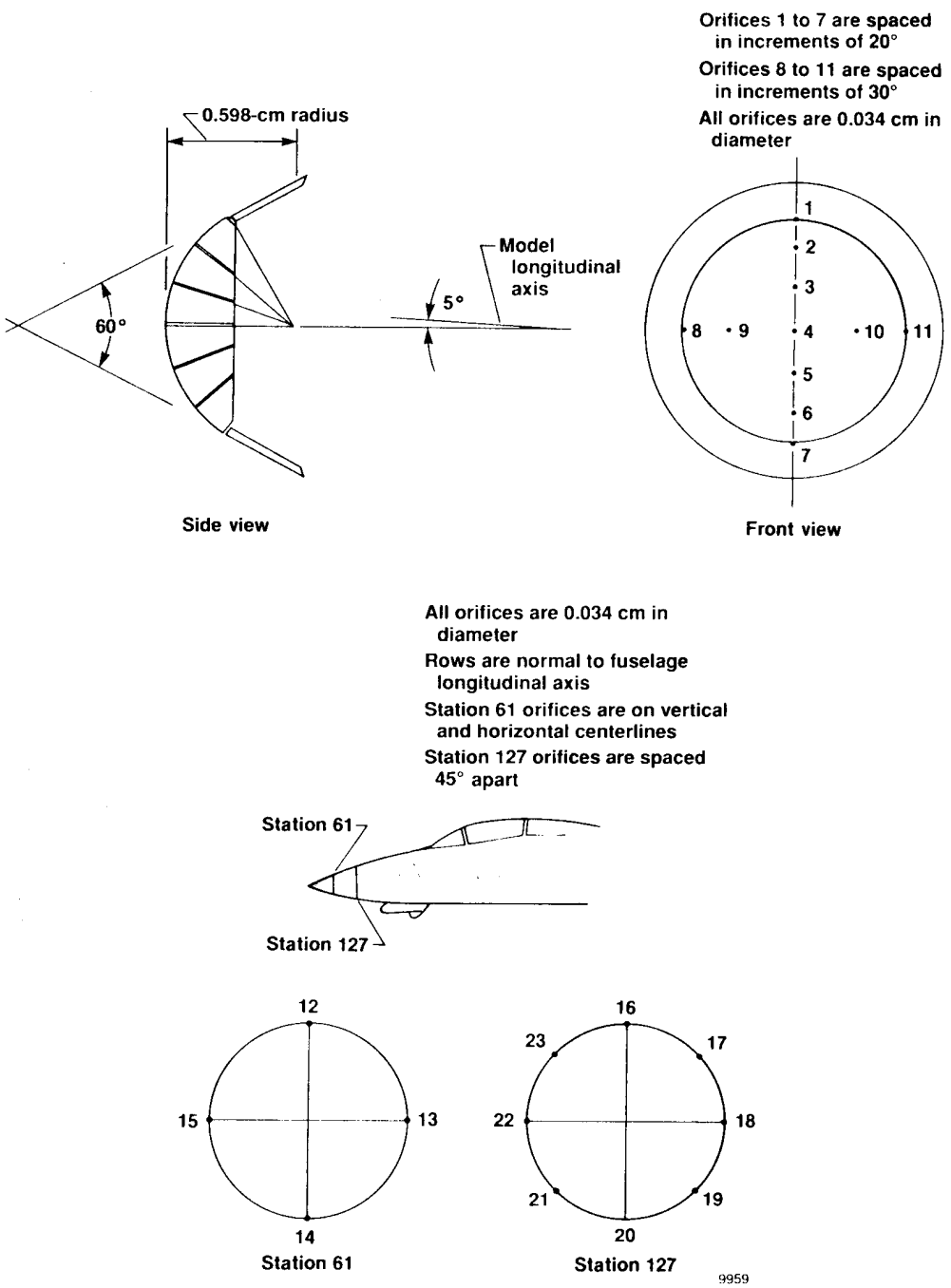

Figure 2. Locations of FADS nose cap and fuselage station orifices.

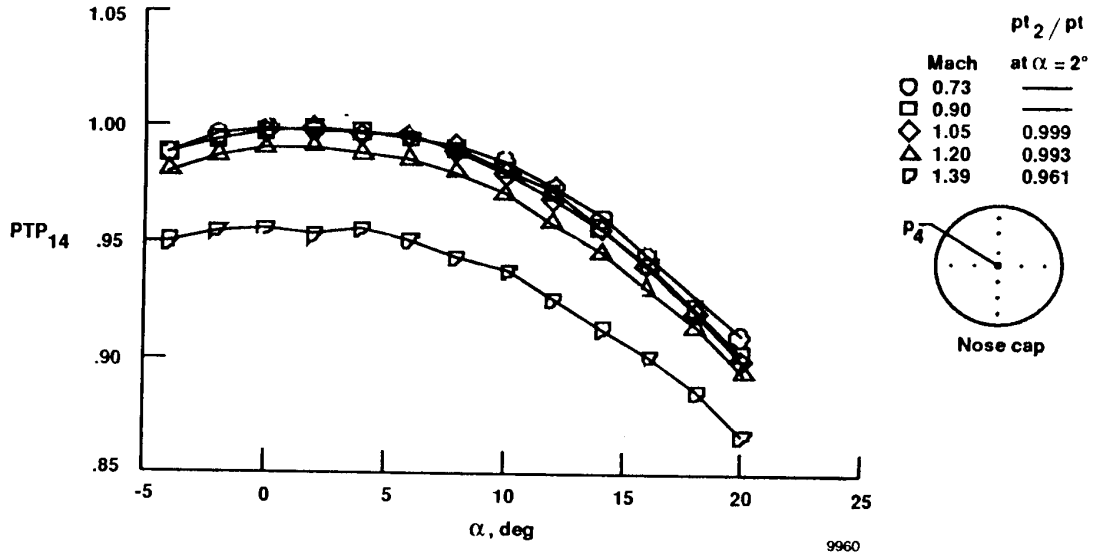

(a) Parameters PTP_{14}.

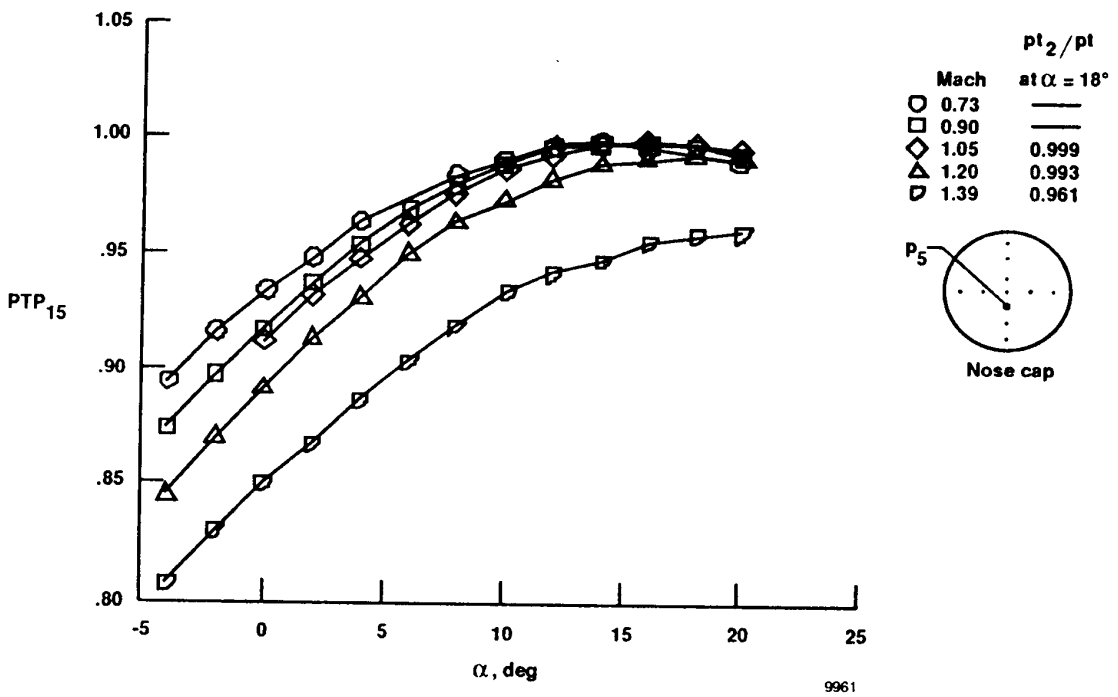

(b) Parameters PTP_{15}.

Figure 3. Variation of stagnation pressure parameters with angle of attack.

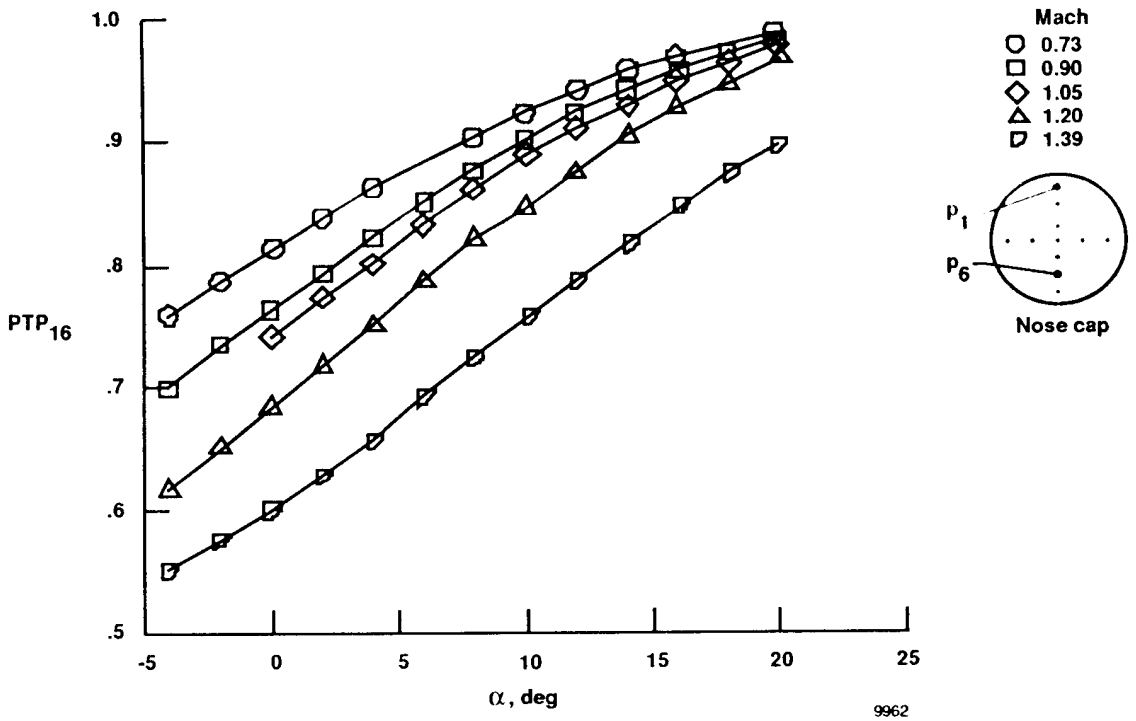

(c) Parameters PTP_{16}.

Figure 3. Concluded.

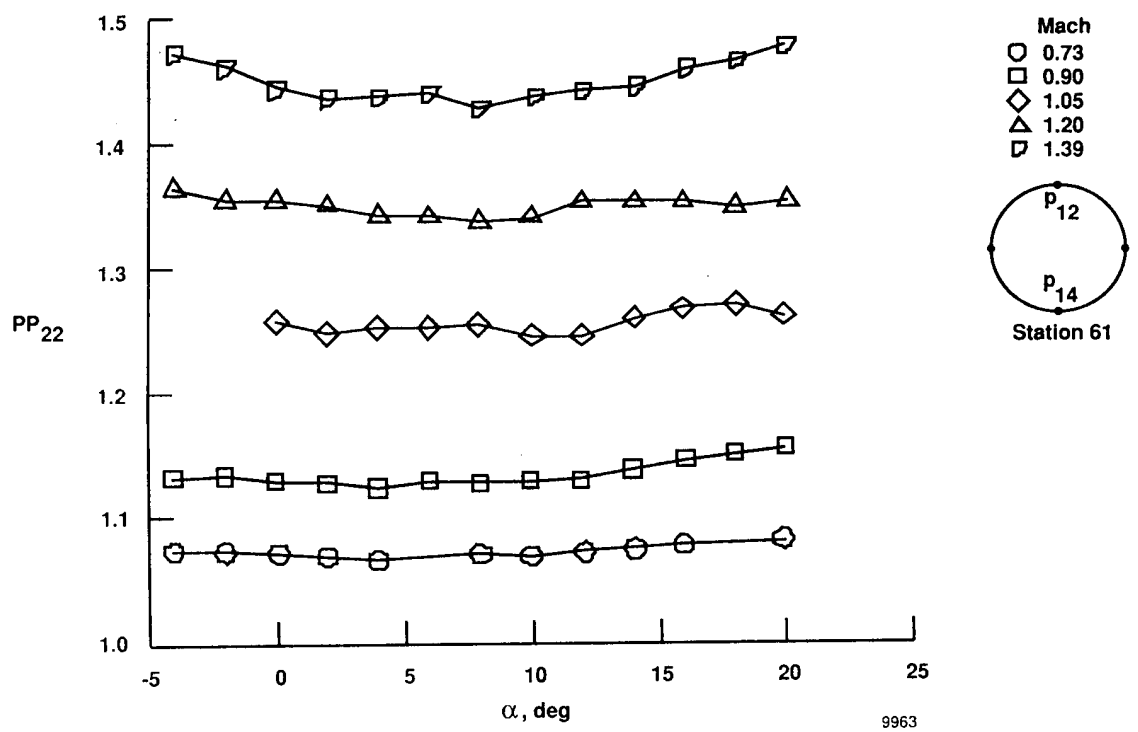

(a) Parameter PP_{22}.

Figure 4. Variation of static pressure parameters with angle of attack.

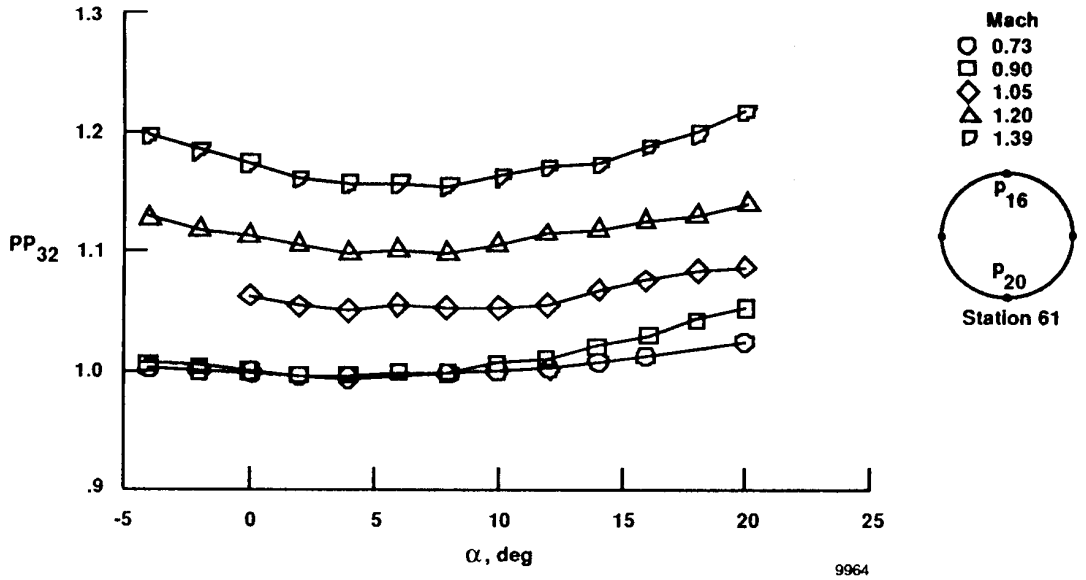

(b) Parameter PP_{32}.

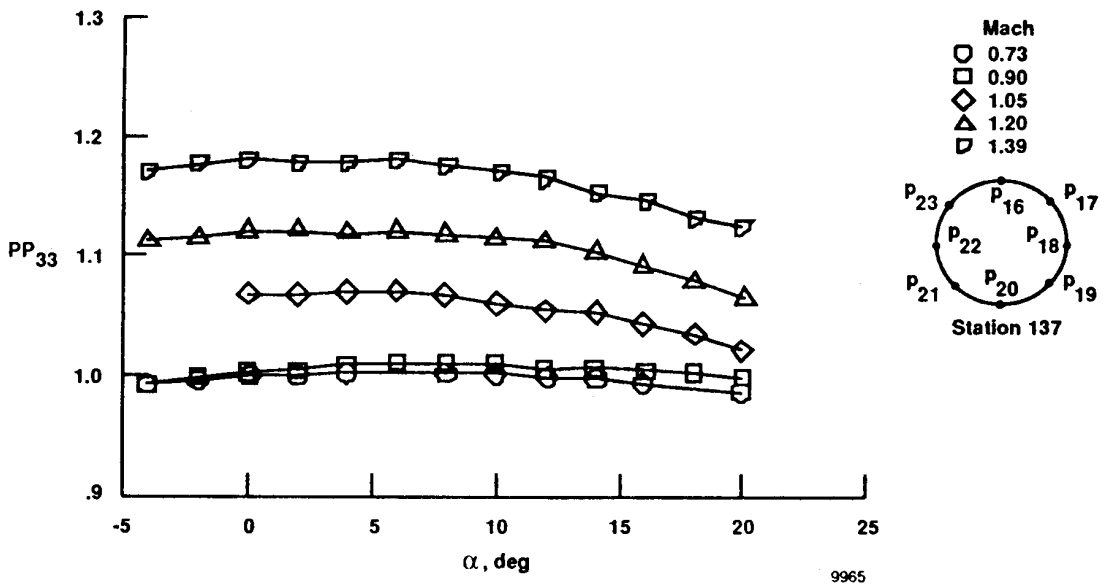

(c) Parameter PP_{33}.

Figure 4. Concluded.

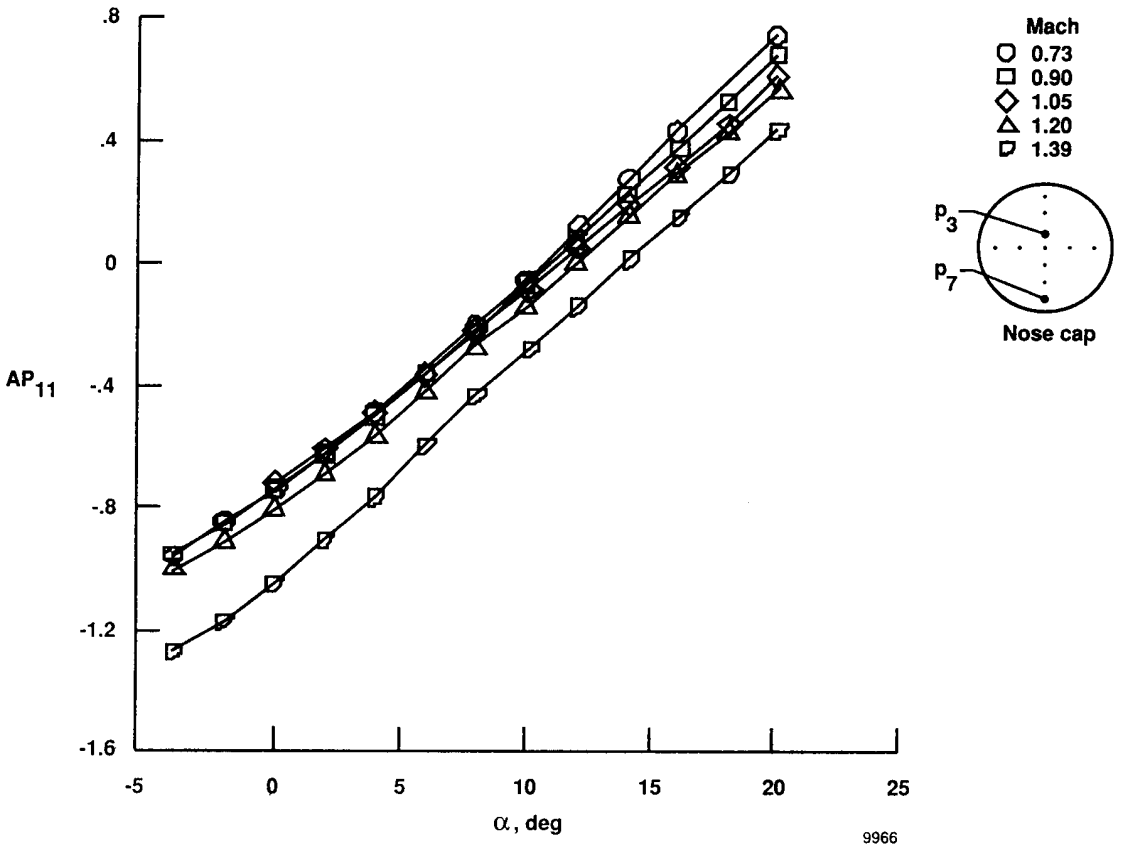

(a) Parameter AP_{11}.

Figure 5. Variation of angle of attack parameters with angle of attack.

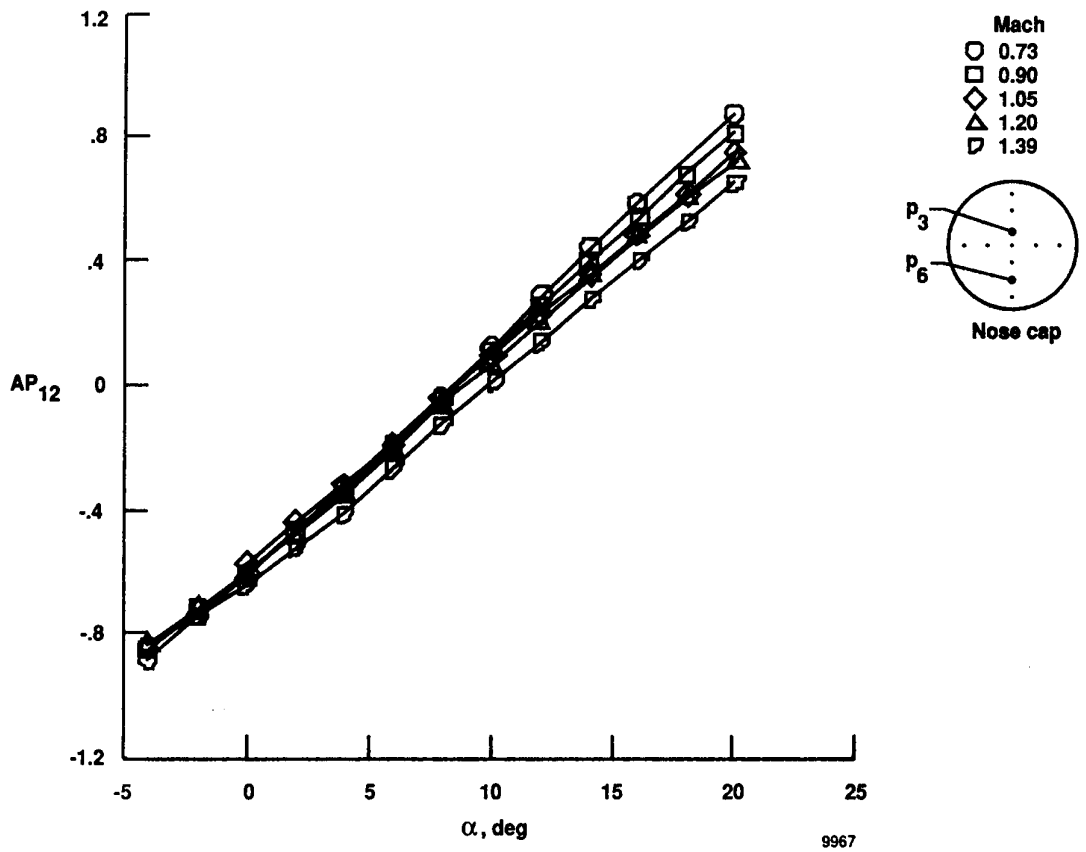

(b) Parameter AP_{12}.

Figure 5. Continued.

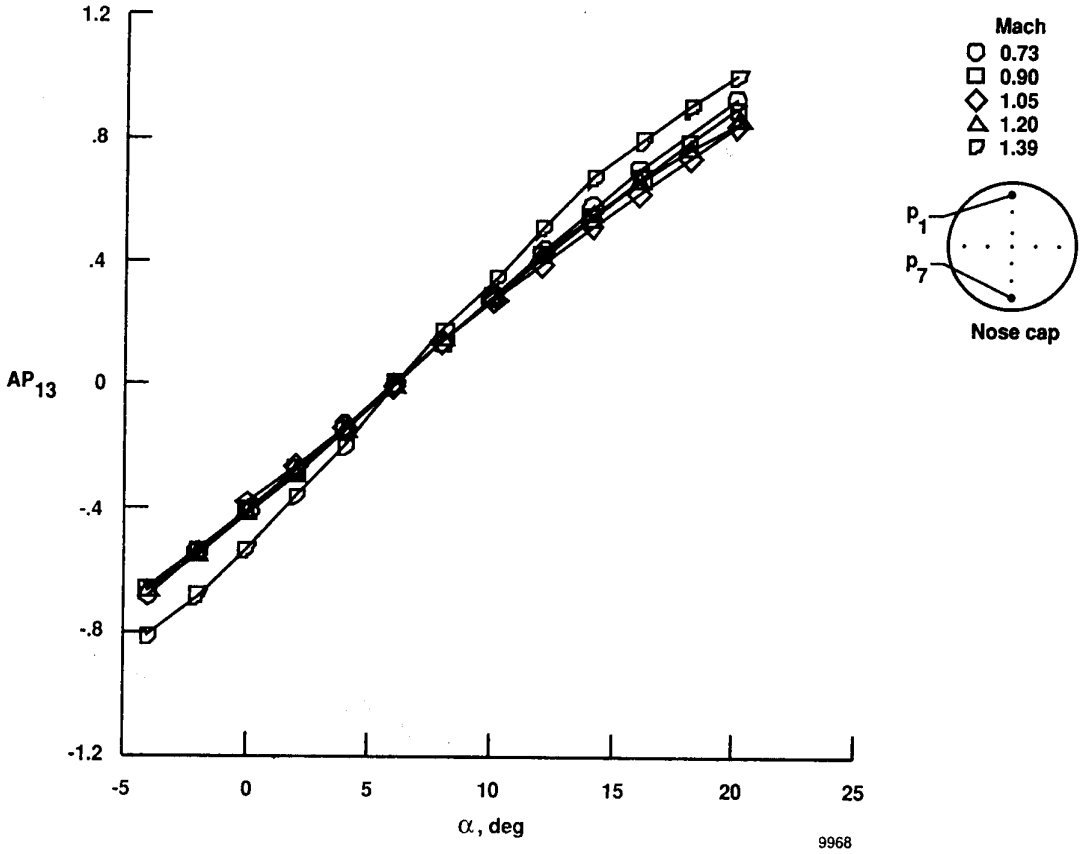

(c) Parameter AP_{13}.

Figure 5. Continued.

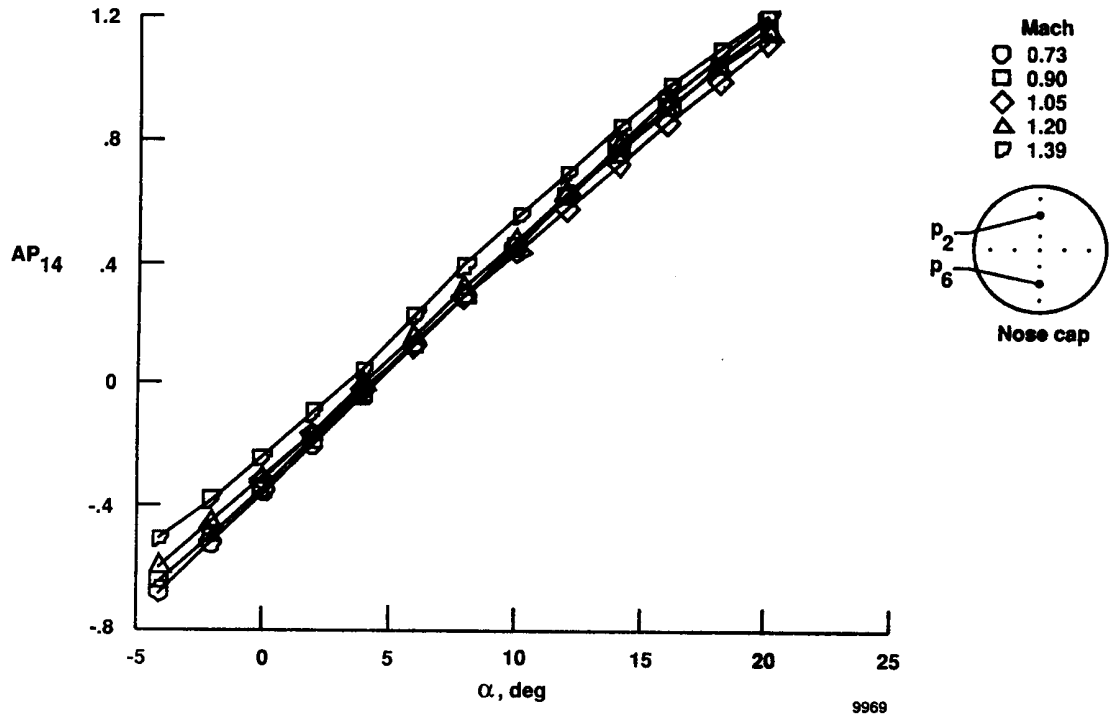

(d) Parameter AP_{14}.

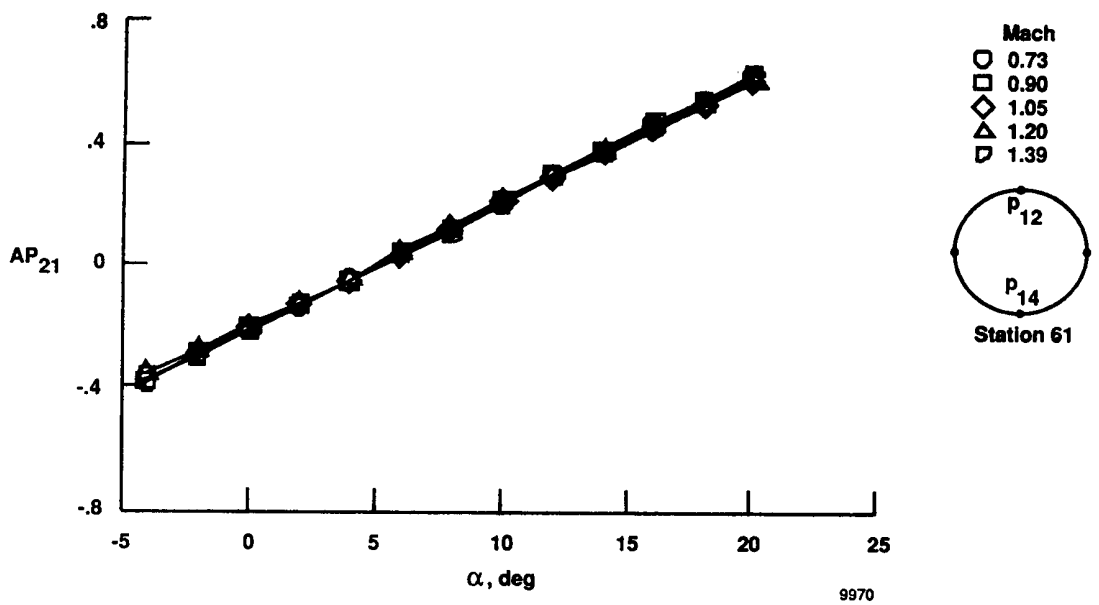

(e) Parameter AP_{21}.

Figure 5. Continued.

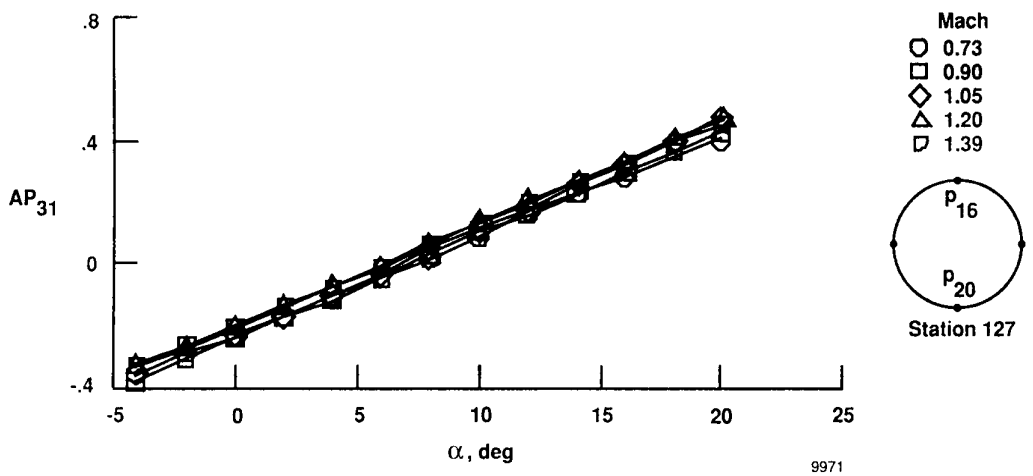

(f) Parameter AP_{31}.

Figure 5. Concluded.

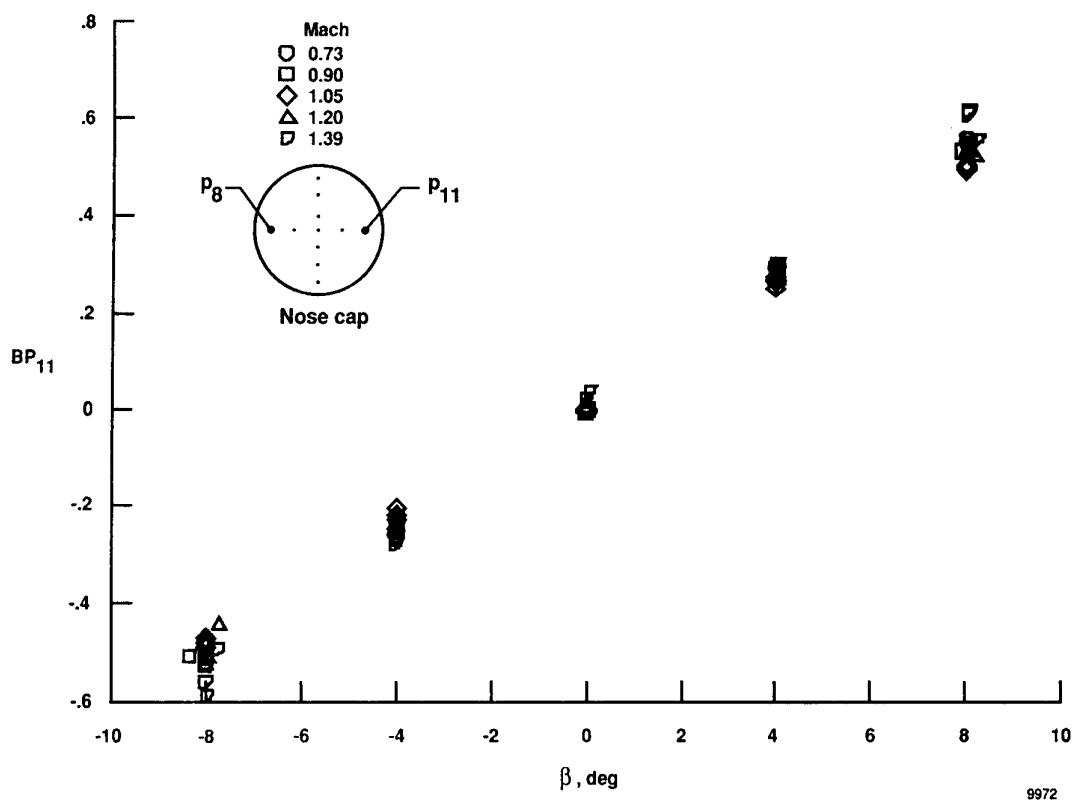

(a) Parameter BP_{11}.

Figure 6. Variation of angle of sideslip parameters with angle of sideslip.

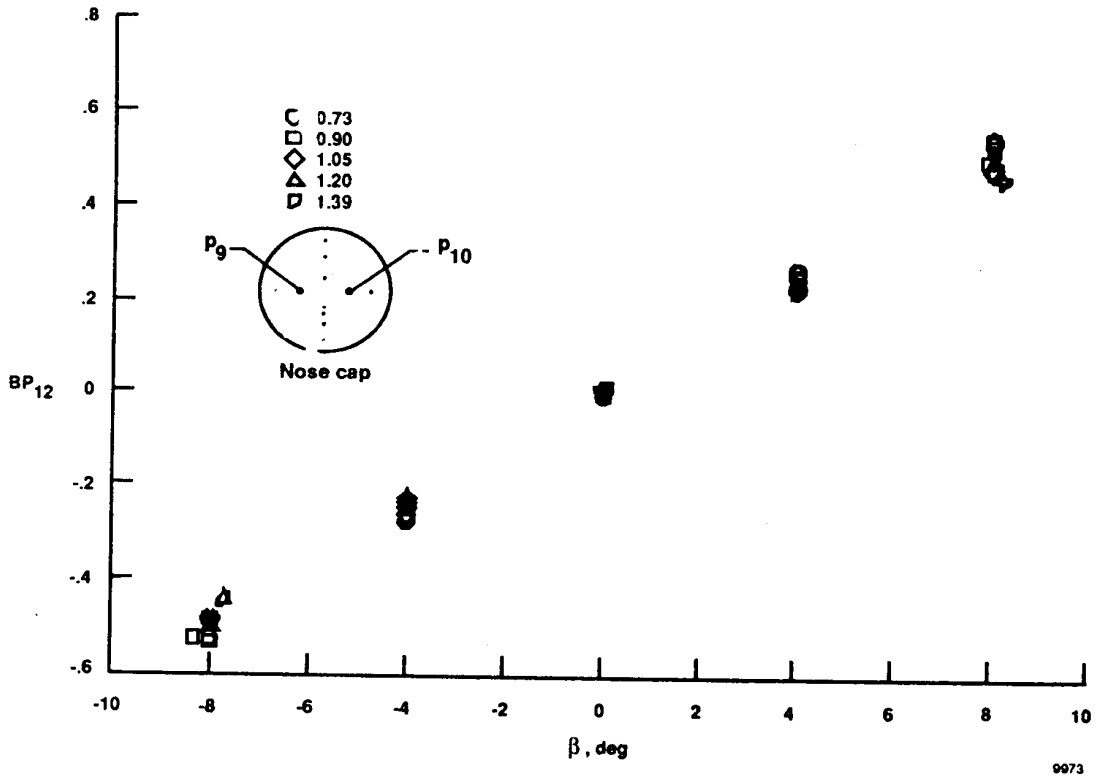

(b) Parameter BP_{12}.

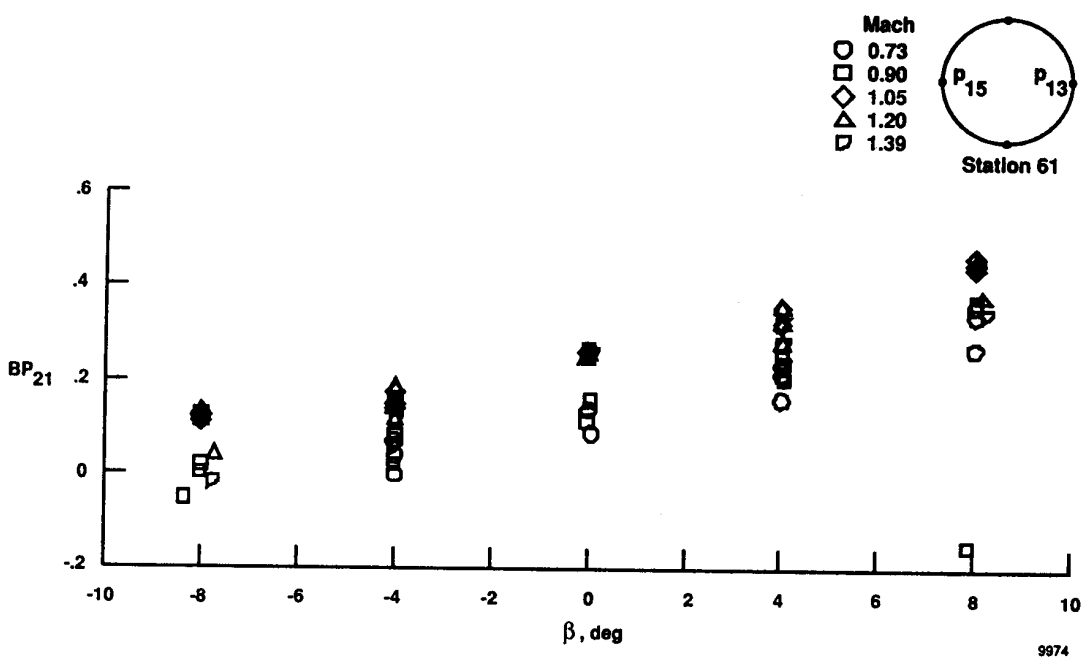

(c) Parameter BP_{21}.

Figure 6. Continued.

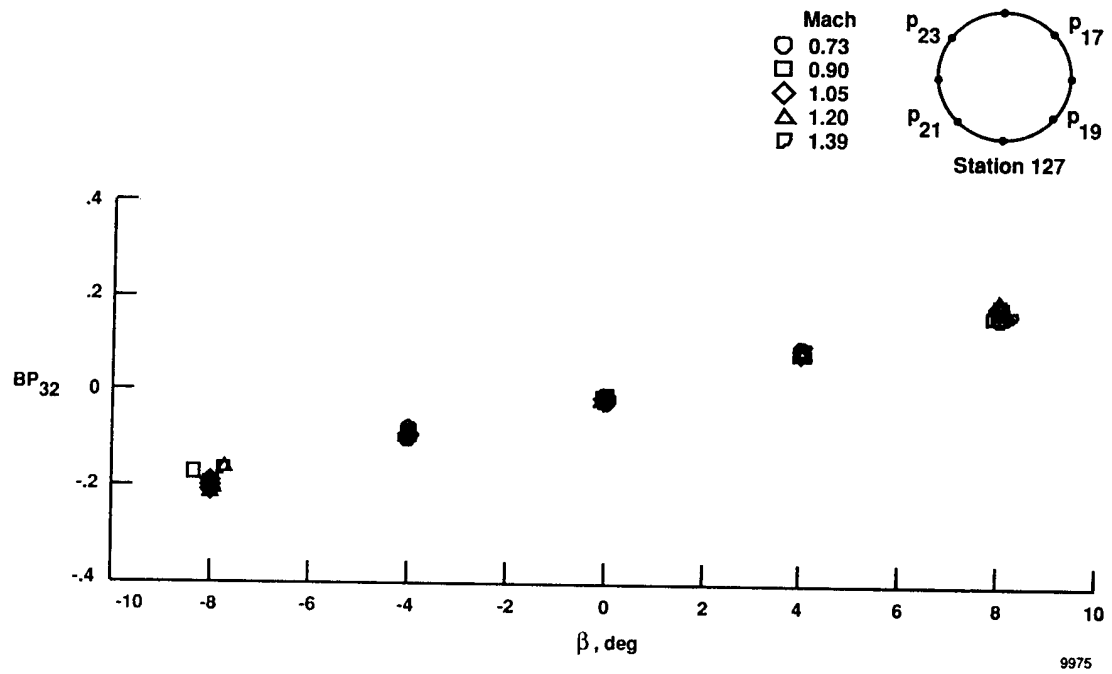

(d) Parameter BP_{32}.
Figure 6. Concluded.

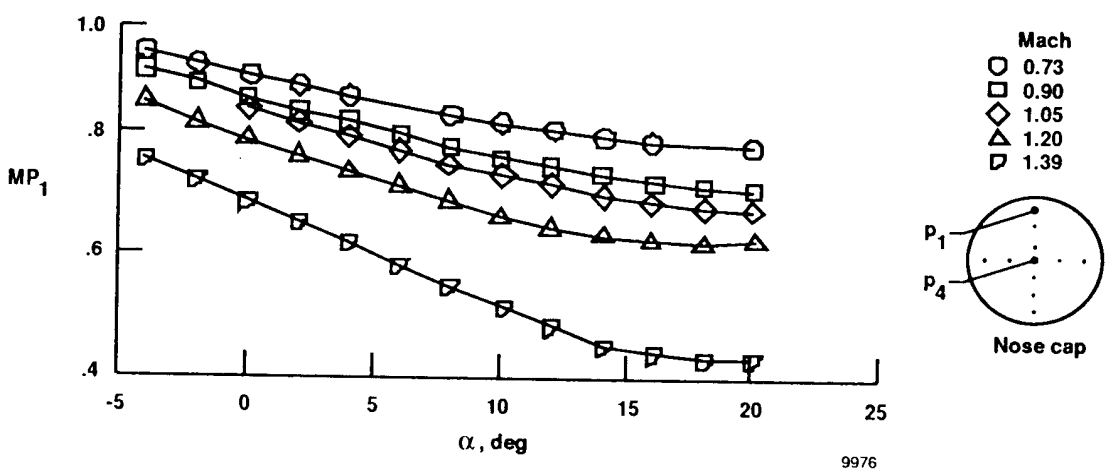

(a) Parameter MP_1.

Figure 7. Variation of Mach number parameters with angle of attack.

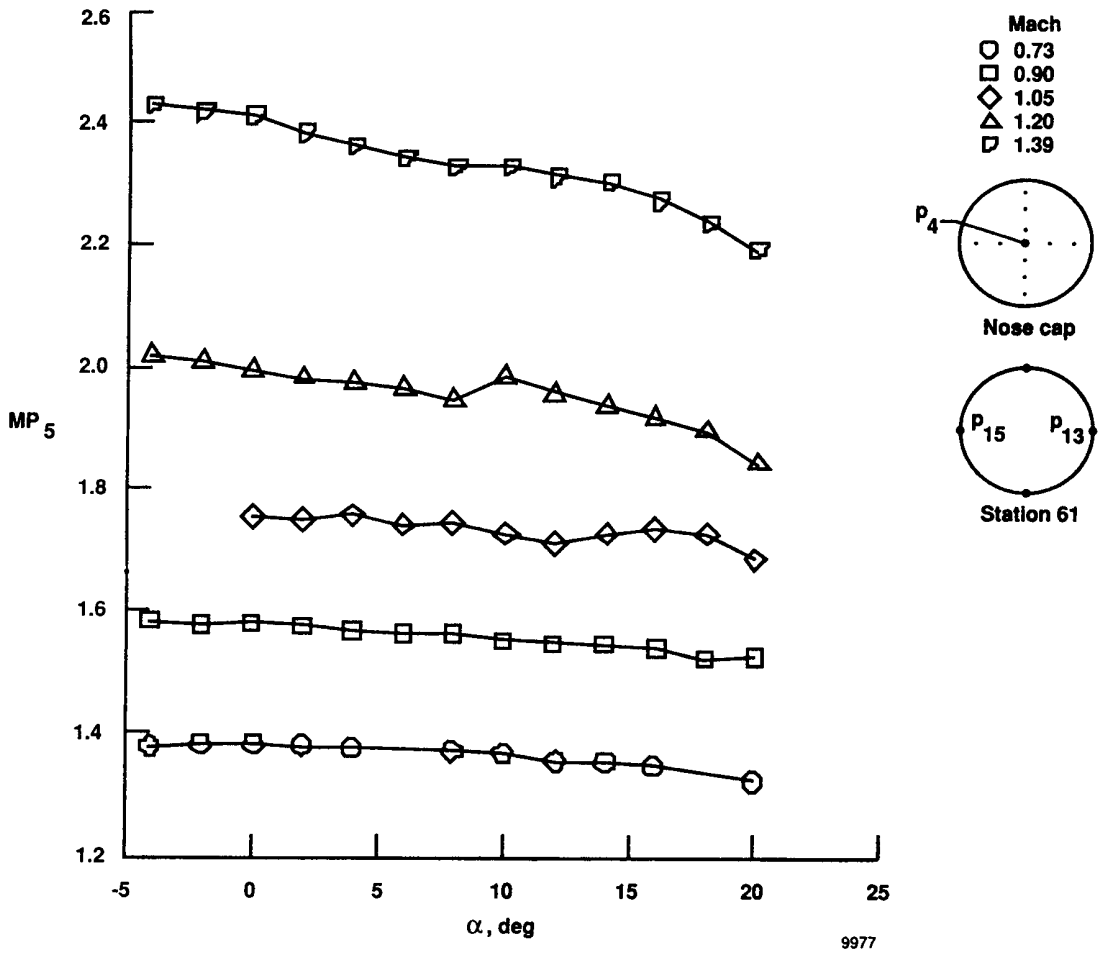

(b) Parameter MP_5.
Figure 7. Continued.

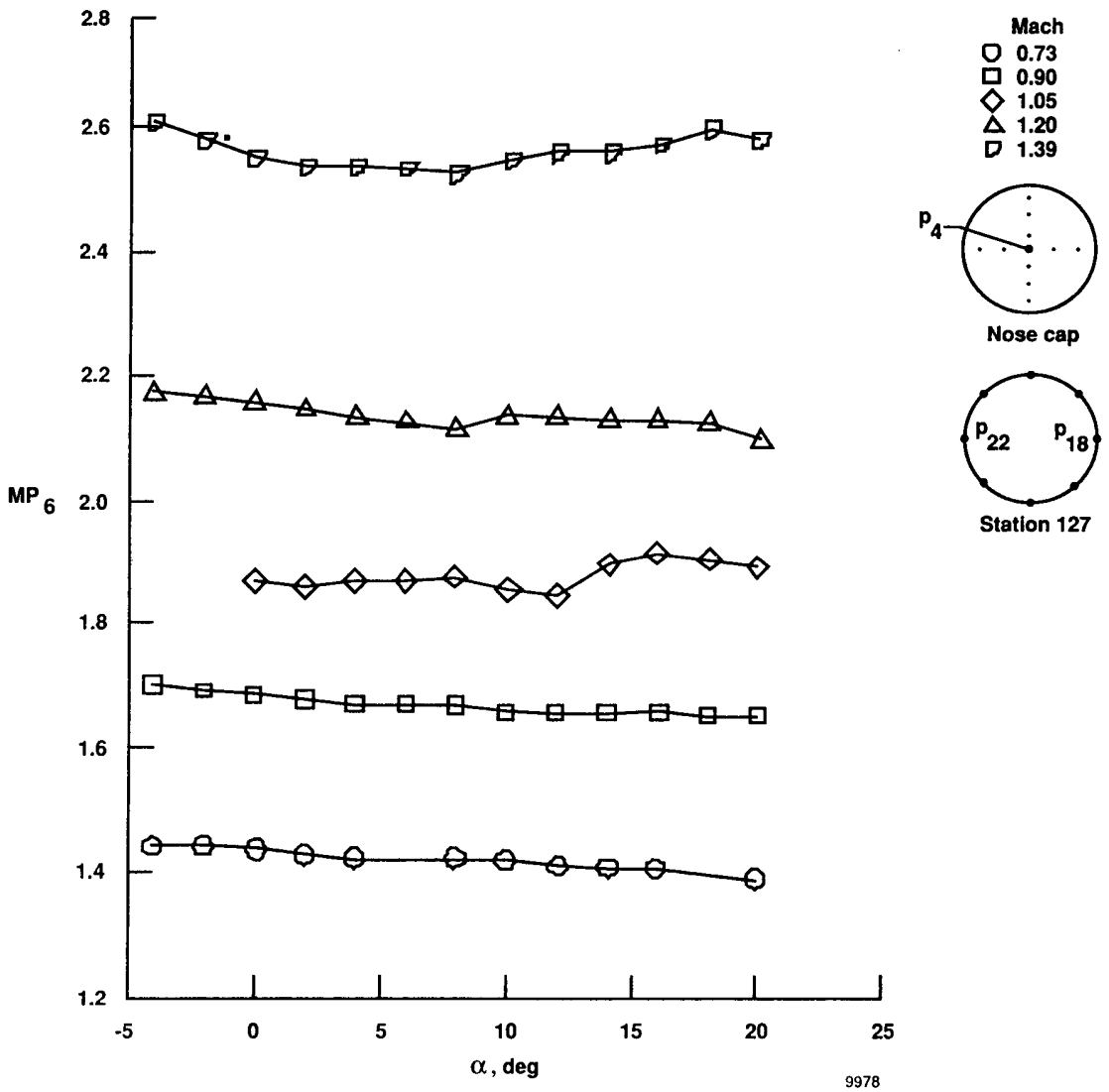

(c) Parameter MP_6.

Figure 7. Concluded.

NASA
National Aeronautics and Space Administration

Report Documentation Page

1. Report No.	2. Government Accession No.	3. Recipient's Catalog No.
NASA TM-101697		

4. Title and Subtitle	5. Report Date
Wind-Tunnel Investigation of a Flush Airdata System at Mach Numbers From 0.7 to 1.4	April 1990
	6. Performing Organization Code
7. Author(s)	8. Performing Organization Report No.
Terry J. Larson, Timothy R. Moes, and Paul M. Siemers III	H-1544
	10. Work Unit No.
9. Performing Organization Name and Address	RTOP 505-6021
NASA Ames Research Center Dryden Flight Research Facility P.O. Box 273, Edwards, CA 93523-0273	11. Contract or Grant No.
	13. Type of Report and Period Covered
12. Sponsoring Agency Name and Address	Technical Memorandum
National Aeronautics and Space Administration Washington, DC 20546	14. Sponsoring Agency Code

15. Supplementary Notes

Terry J. Larson is affiliated with Analytical Mechanics Associates; Paul M. Siemers III is affiliated with Langley Research Center.

16. Abstract

Flush pressure orifices installed on the nose section of a 1/7-scale model of the F-14 airplane were evaluated for use as a flush airdata system (FADS). Wind-tunnel tests were conducted in the 11- by 11-ft Unitary Wind Tunnel at NASA Ames Research Center. A full-scale FADS of the same configuration was previously tested using an F-14 aircraft at the Dryden Flight Research Facility of NASA Ames Research Center (Ames-Dryden). These tests, which have been published, are part of a NASA program to assess accuracies of FADS for use on aircraft. The test program also provides data to validate algorithms for the shuttle entry airdata system developed at the NASA Langley Research Center. The wind-tunnel test Mach numbers were 0.73, 0.90, 1.05, 1.20, and 1.39. Angles of attack were varied in 2° increments from −4° to 20°. Sideslip angles were varied in 4° increments from −8° to 8°. Airdata parameters were evaluated for determination of free-stream values of stagnation pressure, static pressure, angle of attack, angle of sideslip, and Mach number. These parameters are, in most cases, the same as the parameters investigated in the flight test program. The basic FADS wind-tunnel data are presented in tabular form. A discussion of the more accurate parameters is included.

17. Key Words (Suggested by Author(s))	18. Distribution Statement
Airdata Flow-angle measurements Flush airdata system Flush pressure orifices	Unclassified — Unlimited Subject category 06

19. Security Classif. (of this report)	20. Security Classif. (of this page)	21. No. of pages	22. Price
Unclassified	Unclassified	35	A03

NASA FORM 1626 OCT 86

For sale by the National Technical Information Service, Springfield, VA 22161-2171.